

UTILIZING HIGH-PERFORMANCE COMPUTING TO IMPROVE  
PERFORMANCE AND INVESTIGATE SENSITIVITY OF AN  
INVERSION MODEL FOR HYPERSPECTRAL REMOTE SENSING  
OF SHALLOW CORAL ECOSYSTEMS

By

Carolina Gerardino Neira

A thesis submitted in partial fulfillment of the requirements for the degree of  
MASTER OF SCIENCE

in

ELECTRICAL ENGINEERING

UNIVERSITY OF PUERTO RICO  
MAYAGÜEZ CAMPUS

2007

Approved by:

---

James Goodman, Ph.D  
Member, Graduate Committee

---

Date

---

Miguel Velez-Reyes, Ph.D  
Member, Graduate Committee

---

Date

---

Wilson Rivera-Gallego, Ph.D  
President, Graduate Committee

---

Date

---

Omar Colon-Reyes, Ph.D  
Representative of Graduate Studies

---

Date

---

Isidoro Couvertier, Ph.D  
Chairperson of the Department

---

Date

Abstract of Thesis Presented to the Graduate School  
of the University of Puerto Rico in Partial Fulfillment of the  
Requirements for the Degree of Master of Science

**UTILIZING HIGH-PERFORMANCE COMPUTING TO IMPROVE  
PERFORMANCE AND INVESTIGATE SENSITIVITY OF AN  
INVERSION MODEL FOR HYPERSPECTRAL REMOTE SENSING  
OF SHALLOW CORAL ECOSYSTEMS**

By

Carolina Gerardino Neira

2007

Chair: Wilson Rivera-Gallego

Major Department: Electrical and Computer Engineering

This research presents a sensitivity analysis of a semi-analytical inversion model for hyperspectral remote sensing of shallow coral ecosystems. Using this inversion model, five parameters describing water column biooptical properties, bathymetry and magnitude of bottom reflectance are retrieved. In addition to the parameters of interest, the model contains 12 nuisance parameters that are traditionally assigned a fixed set of values. A sensitivity analysis of estimates retrieved to these nuisance parameters is accomplished using SimLab software to study their impact on model output. The computationally intensive analysis was enabled implementing the inversion model within a parallel processing framework using GENCAN. The sensitivity analysis was used to identify which nuisance parameters are most influential on the parameters of interest. The nuisance parameters found to be most relevant are:  $S$ , the spectral slope of the absorption coefficient for gelbstoff,  $Y$ , the spectral power coefficient for calculating the backscattering coefficient, and  $D_{op}$ , a constant in the equation for the distribution function for scattered photons from the bottom.

Resumen de Tesis Presentado a Escuela Graduada  
de la Universidad de Puerto Rico como requisito parcial de los  
Requerimientos para el grado de Maestría en Ciencias

**UTILIZANDO COMPUTACIÓN DE ALTO-RENDIMIENTO PARA  
MEJORAR EL DESEMPEÑO E INVESTIGAR SENSITIVIDAD DE  
UN MODELO DE INVERSIÓN PARA PERCEPCIÓN REMOTA  
HIPERESPECTRAL EN ECOSISTEMAS DE CORAL EN AGUAS  
POCO PROFUNDAS**

Por

Carolina Gerardino Neira

2007

Consejero: Wilson Rivera-Gallego  
Departamento: Ingeniería Eléctrica y Computadoras

Esta investigación presenta un análisis de sensibilidad aplicado a un modelo semi-analítico inverso, para imágenes hiperespectrales de ecosistemas de aguas poco profundas. El modelo de inversión encuentra cinco parámetros de interés los cuales describen propiedades bio-ópticas de la columna de agua, profundidad y reflectancia del fondo marino. Adicionalmente, el modelo tiene 12 parámetros nuisance, cuyos valores son tradicionalmente fijados. Se utilizó el software SimLab para un análisis de sensibilidad de los estimados de los parámetros nuisance y ver su impacto en la salida del modelo. El complejo análisis computacional fue posible implementando el modelo de inversión en una infraestructura para procesamiento en paralelo utilizando el método GENCAN. El análisis de sensibilidad permitió encontrar los parámetros nuisance más influyentes en los parámetros de interés. Los parámetros nuisance más importantes son:  $S$ , la pendiente espectral del coeficiente de absorción para gelbstoff,  $Y$ , la potencia espectral del coeficiente de retrodispersión, y  $D_{op}$ , constante en la función de distribución por fotones dispersos desde el fondo.

To my parents and siblings for their love in the distance.

To Fabian for his sapience, support and unconditional love.

Thanks

## ACKNOWLEDGMENTS

I would like to express my gratitude to my advisor, Dr. Wilson Rivera, for giving me the opportunity to work in this research and for his support during these years. To Dr. James Goodman, because the distance was not an impediment to be always at my side giving me all his support and guidance and for showing me how beautiful is the sea. To Dr. Miguel Velez, for his time and explanations; thanks for helping me find the way to finish this research. To my committee thanks for your trust in me and my work.

I also want to thank the staff and group of CenSSIS, Marie, Samuel, Ricardo, Maribel, Claribel and Vanessa, for their great support and friendship, and my partners at the lab, especially Carlos Rivera for the days with just the sound of a click; to PDCLab for admitting me in your family, Mariana, John, Cesar, Kennie and Fernando. Thanks also to the DSP group for the long nights that we shared, to Checho and Fabian. Thanks to my friends who always shared my triumphs and falls, to Lolix, Maria, Orisnella, Miguel, Lissette, Wilson, Katrina, Chely, Gerardo, Arjuna, Aponte, Alexandra y Maria Elena. Thanks to the staff of the International office, Gildreth, Mirna, Ilia and Mariela, for receiving me in Puerto Rico with open arms. I would like to thank a very especial person, Sandy, for her love and patience; there is not a person greater than you.

I would like to thank God for giving me the courage, patience and faith during my residence here in Puerto Rico, I am thankful for putting in my path the correct and beautiful people during this journey. Finally, I want to express my gratitude to all the people that, direct or indirectly, helped me in any way so I could finish my master and have a great experience along the way.

This work was supported in part by CenSSIS, the Center for Subsurface Sensing and Imaging Systems, under the Engineering Research Centers Program of the National Science Foundation (Award Number ECE-986821). This work was also supported by NASA Training Grant NNG05GG78H (PR Space Grant) and NASA Cooperative Agreement NNX07AO30A (PR NASA EPSCoR).

## TABLE OF CONTENTS

	<u>page</u>
ABSTRACT ENGLISH . . . . .	ii
ABSTRACT SPANISH . . . . .	iii
ACKNOWLEDGMENTS . . . . .	vi
LIST OF TABLES . . . . .	x
LIST OF FIGURES . . . . .	xi
LIST OF ABBREVIATIONS . . . . .	xiii
LIST OF SYMBOLS . . . . .	xiv
<b>1 INTRODUCTION . . . . .</b>	<b>1</b>
1.1 Overview . . . . .	1
1.2 Problem statement . . . . .	3
1.3 Solution Approach . . . . .	3
1.4 Research Objectives . . . . .	4
1.5 Contributions . . . . .	5
1.6 Thesis Structure . . . . .	5
<b>2 PRELIMINARY CONCEPTS AND RELATED WORK . . . . .</b>	<b>6</b>
2.1 Remote Sensing . . . . .	6
2.1.1 Energy Interaction process . . . . .	8
2.2 Remote Sensing Algorithms . . . . .	11
2.2.1 Hydrolight Model . . . . .	11
2.2.2 Semi-analytical Inversion Model . . . . .	12
2.3 Sensitivity Analysis . . . . .	13
2.4 Parallel Computing . . . . .	15
2.4.1 Parallel architectures . . . . .	16
2.4.2 Message Passing Interface (MPI) . . . . .	17
<b>3 SEMI-ANALYTICAL INVERSION MODEL . . . . .</b>	<b>19</b>
3.1 Mathematical Foundation of the SAI model . . . . .	19
3.1.1 Nuisance Parameters . . . . .	25
3.1.1.1 Spectral slope of $a_g$ (S) . . . . .	26
3.1.1.2 Spectral shape parameter (Y) . . . . .	26

	3.1.1.3	Constants of $b_{bw}$	27
	3.1.1.4	Constants of $D_u^C$	27
	3.1.1.5	Constants of $D_u^B$	28
	3.1.1.6	$g_o$ and $g_1$	28
	3.1.1.7	$\zeta$ and $\Gamma$	28
3.2		Synthetic data for experiments	29
4		PARALLEL IMPLEMENTATION OF SAI MODEL AND EXPERIMENTAL RESULTS	31
4.1		Implementation of SAI model within a Parallel Processing Framework	31
4.2		Non-linear constrained optimization	33
4.3		Results of Optimization Routine Test	37
4.4		Performance Results	44
5		SENSITIVITY ANALYSIS	46
5.1		Sobol Method	46
5.2		Methodology	48
5.3		Results	49
	5.3.1	Results for Clear Water	49
	5.3.2	Results for Optically Dense Water	57
6		CONCLUSIONS AND FUTURE WORKS	64
6.1		Conclusions	64
6.2		Future work	66

LIST OF TABLES

<u>Table</u>		<u>page</u>
3.1	Definition of parameters, [1], [2] . . . . .	20
3.2	Spectral data for absorption parameters . . . . .	24
3.3	Initial values for clear and optically dense water and range of parameters of interest . . . . .	29
5.1	Results for Clear Water with different water depths, H . . . . .	53
5.2	Results for Optically Dense Water with different depths, H . . . . .	59

## LIST OF FIGURES

<u>Figure</u>	<u>page</u>
2.1 Electromagnetic Spectrum, Image Courtesy of [3] . . . . .	6
2.2 Hyperspectral Imaging, Figure reprinted from "Spectral Image for Remote Sensing," [4] . . . . .	7
2.3 Interactions of EMR, Image Courtesy of [3], [5] . . . . .	9
2.4 Interactions of EMR with different surface materials, Image Courtesy of [3] . . . . .	10
2.5 Scheme of a parallel problem [6] . . . . .	16
4.1 Implementation of the semi-analytical model as a forward and inverse model . . . . .	32
4.2 Percent Errors for IDL and GENCAN optimization methods for clear water . . . . .	38
4.3 Percent Errors for IDL and GENCAN optimization methods for clear water, continuation . . . . .	39
4.4 Percent Errors for IDL and GENCAN optimization methods for clear water, continuation . . . . .	40
4.5 Percent Errors for IDL and GENCAN optimization methods for optically dense water . . . . .	41
4.6 Percent Errors for IDL and GENCAN optimization methods for optically dense water, continuation . . . . .	42
4.7 Percent Errors for IDL and GENCAN optimization methods for optically dense water, continuation . . . . .	43
4.8 Execution time of SAI model for clear water (a); enlarge subset (b) . . . . .	44
4.9 Speedup of SAI model for clear water . . . . .	45
5.1 Steps to accomplish the Sensitivity Analysis . . . . .	49
5.2 Results of uncertainty analysis for clear water at 5 meters . . . . .	51
5.3 Results of uncertainty analysis for clear water at 10 meters . . . . .	52

5.4	Main results of the sensitivity analysis for clear water . . . . .	55
5.5	Results of total sensitivity index for parameter H for clear water at 30 meters depth . . . . .	56
5.6	Results of total sensitivity index for clear water at 5 and 30 meters depth . . . . .	56
5.7	Results of uncertainty analysis for optically dense water at 1 meter . .	58
5.8	Principal results of sensitivity analysis for optically dense water . . .	61
5.9	Results of total sensitivity index for optically dense water at 5 and 30 meters depth . . . . .	62
5.10	Comparison of first and second order effects for optically dense water at 5 meters depth . . . . .	63

## LIST OF ABBREVIATIONS

AVIRIS	Airborne Visible/Infrared Imaging Spectrometer
CC-UMA	Cache Coherent Uniform Memory Access
CC-NUMA	Cache Coherent Non Uniform Memory Access
CG	Conjugate Gradient
CDOM	Colored Dissolved Organic Matter
EMR	Electromagnetic Radiation
ENVI	Environment for Visualizing Images
FAST	Fourier Amplitude Sensitivity Test
HPF	High Performance Fortran
IDL	Iterative Data Language
LAM-MPI	Local Area Multicomputer Message Passing Interface
MIMD	Multiple Instruction Multiple Data
MISD	Multiple Instruction Single Data
MPI	Message Passing Interface
NIR	Near Infrared
NUMA	Non Uniform Memory Access
OOL	Open Optimization Library
POXIS	Portable Operating System Interface
PVM	Parallel Virtual Machine
SA	Sensitivity Analysis
SAI	Semi-Analytical Inversion
SIMD	Single Instruction Multiple Data
SimLab	Simulation Environment for Uncertainty and Sensitivity Analysis
SISD	Single Instruction Single Data
SMP	Symmetric Multiprocessor Machines
SPG	Spectral Projected Gradient
ST	Sensitivity Total index
SWIR	Short Wavelength Infrared
UA	Uncertainty Analysis
UMA	Uniform Memory Access
UPC	Unified Parallel C
VIS	Visible Spectrum

## LIST OF SYMBOLS

m	meter.
nm	nanometer.
rad	radian (plane angle)
Sr	Steradian (solid angle).

# CHAPTER 1

## INTRODUCTION

### 1.1 Overview

Remote sensing is being utilized for both qualitative visual overviews and the quantitative systematic assessment and monitoring of coral ecosystems in shallow waters. Hyperspectral remote sensing, in particular, is being used to study shallow waters because it offers more spectral detail than multispectral imagery. Components such as phytoplankton, inorganic particles and dissolved organic material make the analysis of coastal water properties, as well as its associated bottom features, more complicated. To study this complex environment, more spectral detail is necessary than that provided by multispectral sensors. Hyperspectral imagery [7], which provides this greater detail, is comprised of information from many contiguous bands of the spectrum. This detail also assists with improving efforts at atmospheric compensation and the removal of sunglint [4].

Quantitative remote sensing of shallow coral water is often supported by empirical, analytical and semi-analytical models, which are used to retrieve information about benthic characteristics and water properties. Empirical models are based on observed relationships between remote sensing reflectance spectra and measured environment properties, while analytical and semi-analytical models are simplified representations of physical relationships (e.g. radiative transfer equations using single or quasi-single scattering theory) [8]. These models define the relationship between

measured surface reflectance and the underlying water properties and benthic characteristics. Where feasible, these models are inverted so that these environmental properties can be extracted from the remote sensing imagery.

Hydrolight [9] is an example of a radiative transfer model that explicitly computes the spectral radial distribution within the water column based on the water properties and benthic composition. This model, which requires numerous parameters, is computationally expensive, making it difficult to use it in an inversion procedure for remote sensing analysis. Semi-analytical models, on the other hand, work with fewer parameters than their analytical counterparts. This is typically accomplished using a number of empirically derived parameters, which are referred to here as nuisance parameters. Although the reduction of parameters is performed to reduce the complexity of the problem, the nuisance parameters still have physical significance and are an integral part of the overall model. The influence of nuisance parameters on retrieval performance is one of the main objective of this study.

The model used for this study is a semi-analytical inversion (SAI) model developed by Lee et al. [1], [2] that retrieves water optical properties, bathymetry and bottom albedo as a function of surface remote sensing reflectance. This SAI model retrieves six environmental parameters,  $P$ ,  $G$ ,  $BP$ ,  $B$ ,  $H$ ,  $\Delta$  (defined in Chapter 3), by minimizing an error function (objective function) that describes the difference between modeled and measured surface reflectance. The same SAI model was adapted by Goodman [5] in IDL (Interactive Data Language)/ENVI [10], [11], as the basis for a benthic unmixing model using hyperspectral imagery from Kaneohe Bay, Hawaii. Goodman solved essentially the same SAI model as developed by Lee et al., but used a slightly modified objective function and only retrieved five parameters (i.e.,  $P$ ,  $G$ ,  $BP$ ,  $B$  and  $H$ ). It is important to note that the values of the nuisance parameters within the model defined by Lee, and used successfully by Goodman in Kaneohe Bay, are not specifically from Hawaii. Therefore, it is assumed that some

of the residual errors found by Goodman are a function of the nuisance parameters.

## 1.2 Problem statement

The values for the nuisance parameters in the semi-analytical inversion (SAI) model developed by Lee et al. were derived using a combination of field observations and Hydrolight simulations. Model testing and validation was completed using data from the west Florida shelf, Key West Florida, and the Bahamas. From this testing, Lee et al. [2] concluded that the model was applicable to normal relatively clear coastal water, but not for extreme cases with more optically dense water, such as the Florida Bay. To evaluate the model in other shallow water conditions, Goodman [12] used imagery from Kaneohe Bay, with areas of known bathymetry and bottom properties but only limited knowledge of measured absorption coefficients and other water properties. Results demonstrated successful application of the model, but also indicated needs for further improvement.

Following the same modeling approach as Goodman, the objective of this study is to use high performance computing to investigate the impact of the nuisance parameters on the variability of the five parameters of interest. High performance computing is used because the sensitivity analysis requires a large number of simulations to evaluate the impact of the nuisance parameters. A parallel implementation is utilized to significantly decrease computation time and thus perform a thorough sensitivity analysis.

## 1.3 Solution Approach

Both an uncertainty analysis (UA) and sensitivity analysis (SA) are used to identify the most influential nuisance parameters and analyze their impact on model

output. The UA shows the uncertainty in the parameters of interest due to the nuisance parameters and the SA indicates how influential the nuisance parameters are on the parameters of interest, which of causes the most uncertainty. This study uses the Sobol method [13], [14], to perform the uncertainty and sensitivity analysis. Although the Sobol method requires the generation of numerous samples to perform the respective analysis, as mentioned above, the SAI model is implemented within a parallel processing framework to enable evaluation of the large set of samples. The resulting implementation reduces the total runtime, enables efficient memory management of large data, and preserves the load balance of sample processing. Studies by Lugo et. al. [15], Hawick et. al. [16] and Valencia et. al. [17] have demonstrated the reduction in runtime and total memory capacity required for different hyperspectral image processing algorithms using the C programming language and Message Passing Interface (MPI) [18] for parallel processing. The current application uses a similar approach, but with C++ and LAM/MPI [19], which is a high-quality open-source implementation of the MPI.

## 1.4 Research Objectives

The overall goal of this work is to identify the most influential nuisance parameters in the semi-analytical inversion (SAI) model developed by Lee et al. The specific objectives are:

- Implement the existing semi-analytical inversion model within a parallel processing framework;
- Carry out a sensitivity analysis of the SAI model to identify the nuisance parameters that contribute the most variability to the parameters of interest.

## 1.5 Contributions

This study focuses on the parallel implementation of the SAI model and on using a sensitivity analysis to identify the most influential nuisance parameters within the model. The SAI model is an important tool for those interested in mapping and monitoring of shallow coral ecosystems (e.g. oceanographers, ecologists, biologists). Results from the parallel implementation can be used to more efficiently execute the model, and results from the sensitivity analysis can be used to identify areas where the model can be improved. Thus, this study facilitates the improved overall implementation of the SAI model, as well as its ability to retrieve information on water properties, bottom albedo and water depth in shallow areas containing corals, and other associated benthic organisms.

## 1.6 Thesis Structure

This thesis is organized as follows: Chapter 2 provides an overview of remote sensing, sensitivity analysis, and high performance computing. Chapter 3 describes the semi-analytical inversion (SAI) model, including a definition of both the parameters of interest and the nuisance parameters. Chapter 4 presents the SAI model implementation and experimental results. Chapter 5 gives a description of the Sobol method and results from the sensitivity analysis. Finally, chapter 6 contains the conclusions and recommendations for future work.

# CHAPTER 2

## PRELIMINARY CONCEPTS AND RELATED WORK

This chapter presents an introduction to the important concepts on remote sensing, sensitivity analysis and parallel computing.

### 2.1 Remote Sensing

Remote sensing instruments measure reflected and/or emitted electromagnetic radiation (EMR) using aerial and satellite platforms [20].

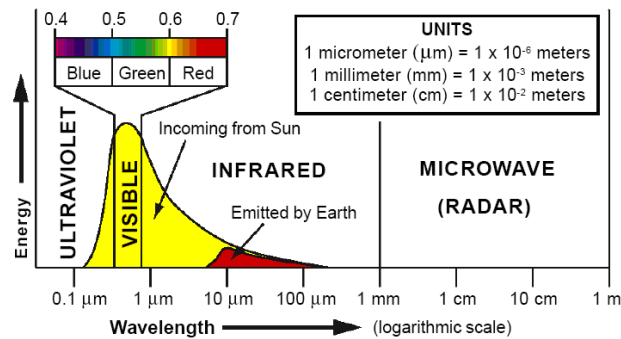


Figure 2.1: Electromagnetic Spectrum, Image Courtesy of [3]

There are two main types of sensors: active and passive sensors. Active sensors are instruments that first illuminate the surface observed using one of many EM probes, and then measure the return signal, while passive sensors detect natural energy reflected or emitted from the object. For passive instruments, the peak solar energy is in the wavelength range of visible light (400 - 700 nm), as shown in Figure

2.1. Other substantial fractions of incoming solar energy appear in the ultraviolet and infrared, with small amounts in the microwave portion of the spectrum.

There are four commonly used categories of remote sensing systems, two that are active and two that are passive [3]: The active systems are imaging radar sensors, which utilize microwave energy, and lidar sensors, which typically utilize lasers in the optical portion of the spectrum. The passive systems are thermal infrared sensors, which detect emitted and reflected thermal radiation, and passive solar radiation sensors, which detect sunlight reflected from the surface. Images generated by these sensors may in turn consist of one band (panchromatic image), a few bands (multispectral image) or many narrow wavelength bands (hyperspectral image). The hyperspectral information used in this thesis has a spectral resolution of 10 nm, which matches the characteristics of the AVIRIS sensor, a passive hyperspectral instrument.

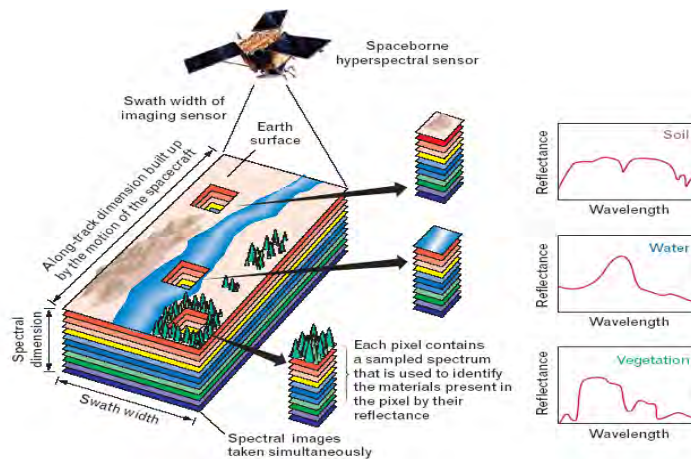


Figure 2.2: Hyperspectral Imaging, Figure reprinted from "Spectral Image for Remote Sensing," [4]

As mentioned in the introduction, hyperspectral sensors offer much greater spectral detail than other traditional sensors, such as panchromatic instruments and multispectral sensors. As a consequence, the spectral properties of individual pixels are obtained in greater detail, which allows a more accurate characterization

of the scene being examined. Figure 2.2 provides an illustration of the differences in spectral detail for three different surface as measured using a hyperspectral instrument. These differences are a function of the chemical composition and physical structure of the material exposed to EMR, which can change the direction, intensity, wavelength content and polarization of EMR. Thus, through an understanding of these relationships, we can characterize the surface material using reflected EMR.

### 2.1.1 Energy Interaction process

Hyperspectral images are collected using imaging spectrometers, which measure upwelling radiance. For areas of shallow water, the measurements of upwelling radiance include scattered skylight, light reflected from the water surface, light reflected from the water column, and light reflected from the bottom. Further, shallow water is typically a heterogeneous environment, with varying amounts of phytoplankton, organic material and inorganic particles in suspension. Thus, the signal is very complex. To analyze these images, apparent reflectance at the water surface is first derived using atmospheric correction models, and sun glint removal algorithms, which are subsequently used to remove the effects of specular reflection at the water surface [21]. Inversion models can then be used to derive information on the properties of the water and the benthic surface.

Figure 2.3 illustrates the interaction process of EMR withing the atmosphere, at the water surface, within the water column and at the bottom. Sunlight first enters the atmosphere (downwelling radiation), interacting with gas molecules, suspended dust particles and aerosols. Portions of this downwelling EMR are scattered and absorbed and the remaining EMR is transmitted to the surface. The resulting surface illumination is a combination of EMR transmitted directly from the Sun and scattered light from other parts of the sky. When the EMR arrives at solid

surface, a portion is absorbed and the rest is reflected back into the atmosphere. However, when this surface is a water surface a portion is still reflected back into the atmosphere, but the remaining EMR is transmitted through the water surface into the water column. The quantity of energy transmitted or reflected at the water surface is dependent on the solar geometry and water surface conditions. Additionally, refraction at the air-water interface alters the incident angles, with light being closer to the vertical plane in the water column than in the air.

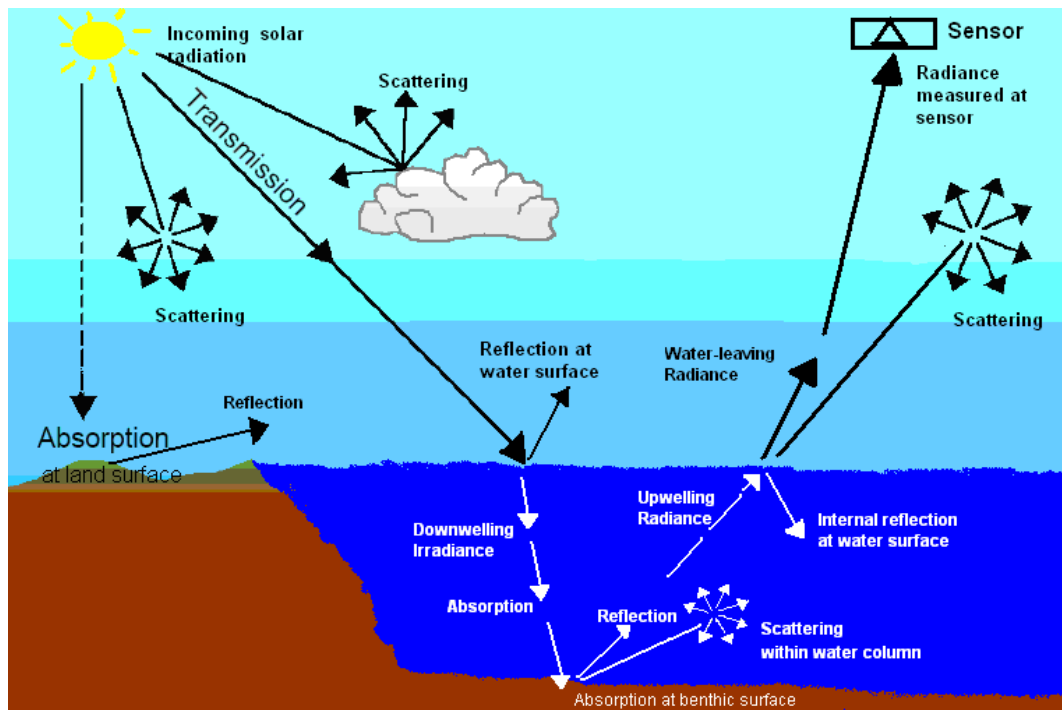


Figure 2.3: Interactions of EMR, Image Courtesy of [3], [5]

As the downwelling EMR passes through the water column it is further subjected to both absorption and scattering. However, note that absorption in the water column is greater at all wavelengths than in the atmosphere, and particularly at wavelengths longer than 800 nm. Upon reaching the bottom, a portion of the energy is absorbed by the benthic surface and the other part is reflected. This reflected energy then experiences the same absorption and scattering in the water column on its way back to the water surface, as well as a similar process at the water surface,

and the upwelling radiance that ultimately leaves the water will experience the same interaction process in the atmosphere as it continues to the sensor to be measured.

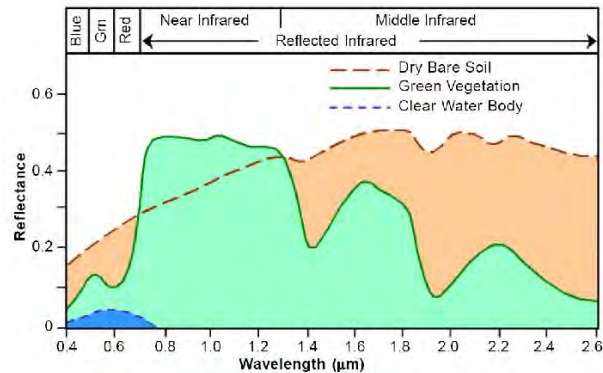


Figure 2.4: Interactions of EMR with different surface materials, Image Courtesy of [3]

The interaction of most importance with respect to classification of bottom composition is the spectral reflectance at the benthic surface. Spectral reflectance, which is the ratio of reflected energy to incident energy as a function of wavelength, is used to characterize the diverse material in the surface. More specifically, as mentioned above, the amount of energy absorbed and reflected at a surface varies for different materials creating a spectral signature that allows its identification. For example, as we can see in Figure 2.4 (and as previously shown in Figure 2.3), water reflects only in one portion of the spectrum (energy at other wavelengths is absorbed), while vegetation and soil reflect energy differently throughout the spectrum. These curves allow the recognition and classification of different surface materials. However, to analyze the bottom reflectance, the water optical properties, water depth and all of the interactions mentioned above must be considered. Additionally, as a limiting factor in the process, the spectral window for performing an analysis of benthic composition [12] is in general limited to the range from 400 to 800 nm [3].

## 2.2 Remote Sensing Algorithms

The energy interaction process is approximated using different physically based modeling approach. As two examples, we have the Hydrolight model which is an accurate solution based on radiative transfer equations, and the SAI model, which includes simplifying assumptions based on empirical data. Both are described below.

### 2.2.1 Hydrolight Model

The fundamental radiative transfer equation [22], representing the radiation transfer processes in media such as water is defined as follows:

$$\mu \frac{dL(\xi, \lambda, z)}{dz} = -c(\lambda, z) L(\xi, \lambda, z) + L_*^E + L_*^I + L_*^S, \quad (2.1)$$

where  $\mu$  is the cosine of elevation angle,  $L$  is the radiance,  $c$  is the total beam attenuation coefficient,  $L_*^E$  is the elastic scattered radiance,  $L_*^I$  is the inelastic scattered radiance, and  $L_*^S$  represents the internal energy sources (e.g., biolumenecence). The variable  $\xi$  is the direction of ray propagation,  $\lambda$  is the wavelength, and  $z$  is the geometrical depth.

The Hydrolight model [9] solves the above time-independent radiative transfer [22] in horizontally homogeneous water with a constant index of refraction. Five principal groups of parameters are input to this model, including the inherent optical properties of the water column, properties of the water substances, the optical reflection and transmission properties of sea surface, which depend on the wind speed and solar angle, the sky spectral radiance distribution, and the spectral properties of the bottom boundary. The inherent optical properties are the scattering coefficient, the absorption coefficient and the scattering phase function. These properties are only dependent on the medium, in this case the water and substances dissolved in it and are not affected by variations in the radiance distribution [8]. The principal

substances considered in the model are the phytoplankton, colored dissolved organic matter (CDOM), and minerals. The input parameters are used to calculate the remote sensing reflectance as a function of depth, angular direction, and wavelength within the seawater. However, as stated earlier, this model is a forward model and not appropriate for inverting the same relationship so that the environmental parameters can be extracted from remote sensing imagery.

### 2.2.2 Semi-analytical Inversion Model

The SAI model is a hyperspectral remote sensing reflectance model for shallow waters developed by Lee et al. [1], [2] to retrieve water optical properties, bathymetry, and bottom albedo from surface reflectance. For shallow waters, the spectral shape of the bottom albedo (i.e., reflectance) is assumed uniform and known. However, the intensity of the bottom albedo can change from place to place.

The SAI calculations center on the prediction of the surface remote sensing reflectance,  $\hat{R}_{rs}$ , which is an apparent optical property defined as the ratio of the water leaving radiance to downwelling irradiance just above the surface. As an apparent optical property,  $R_{rs}$  depends both on the medium, the inherent optical properties, and on the directional structure of the ambient light field. Thus, this quantity varies with respect to the absorption,  $a(\lambda)$ , and backscattering,  $b_b(\lambda)$ , coefficients (inherent optical properties), the bottom albedo,  $\rho(\lambda)$ , water depth,  $H$ , and the solar zenith angle  $\theta_w$ . It is in turn approximated as a function of the subsurface surface remote sensing reflectance,  $\hat{r}_{rs}$ , which is defined as the ratio of upwelling radiance to downwelling radiance evaluated just below the water surface. The relationship between  $\hat{R}_{rs}$  and  $\hat{r}_{rs}$  is defined as:

$$\hat{R}_{rs} = \frac{0.5 r_{rs}}{1 - 1.5 r_{rs}}, \quad (2.2)$$

and the equation for  $\hat{r}_{rs}$  is:

$$r_{rs} = r_{rs}^{dp} \left[ 1 - \exp \left( - \left[ D_u^C + \frac{1}{\cos \theta_w} \right] kH \right) \right] + \frac{1}{\pi} \rho \exp \left( - \left[ D_u^B + \frac{1}{\cos \theta_w} \right] kH \right) \quad (2.3)$$

The left portion on the right side of Equation 2.3 represents the influences from the water column, and the right portion represents the bottom influence. A more complete description of the SAI model is presented in Chapter 3, where the variables and the equations describing the model are discussed in more detail.

Comparisons of the SAI model versus Hydrolight output and field data from Florida both show good agreement [2]. The average error in retrieved water depths between 2 and 20 m was only 5.3% at a wind speed of 5 m/s, and 5.1% at a wind speed of 10 m/s. For average total absorption coefficients at 440 nm ranging from 0.04 and 0.24  $m^{-1}$ , the error was 7% and 6.3% for wind speeds of 5 m/s and 10 m/s, respectively [2]. Therefore, it was concluded that the model produces acceptable results for retrieving water optical properties and water depth.

## 2.3 Sensitivity Analysis

Sensitivity analysis (SA) is “the study of how the uncertainty in the output of a model can be apportioned to different sources of uncertainty in the model input” [23]. Sensitivity analysis has been used in many different fields such as financial applications, risk analysis, signal processing, neural networks, and all the engineering and science areas that work with developments and/or improvements of models. With SA, it is possible to test both different model structures and different values for its variables, as well as explore the behavior and quality of the model. In our case, a research about SA for hyperspectral remote sensing reflectance of shallow waters, is done with SAI model.

The parameters of a model can essentially be divided into two categories, nuisance parameters, which are inputs, and parameters of interest, which are outputs. Thus, SA can be used to determine the uncertainty in the parameters of interest due to the uncertainty in the nuisance parameters [24]. With SA, it is possible to answer questions such as what are the parameters of the system that need further study, what empirical data is most needed for model accuracy and which of the nuisance parameters are the most influential [25] and hence require the most accurate information. SA can be Local or Global. A local SA measures the effect of a given input on a given output, while keeping all other factors in their nominal value and using a small search space. On the other hand, a global SA uses a larger search space and allows all of the input parameters to vary at the same time to measure the effect on a given output factor, thus facilitating analysis of interactions between input factors [24].

The Simulation Environment for Uncertainty and Sensitivity Analysis (SimLab)<sup>1</sup> is a software tool used for performing SA. It has several different analysis methods, including fixed samples, latin hypercube, quasirandom LpTau, Random, Morris, Sobol and Fourier Amplitude Sensitivity Test (FAST). The first four methods are regression based methods, which predict one dependent variable from one or more independent variables. However, these methods all require an assumption of linearity, which is not appropriate for the nonlinear SAI model being examined in this study. This leaves the Morris, Sobol and FAST techniques, which allow for nonlinearity when performing the SA. Morris [24] is a screening method that gives only qualitative output, ranking the nuisance parameters according to their relative influence on the parameters of interest. This measure does not require large numbers of samples and as a consequence is used when the number of input parameters

---

<sup>1</sup> <http://simlab.jrc.cec.eu.int/>

is large and/or the model is computationally expensive. For example, Duarte [26] used the Morris method for analyzing the Hydrolight model. Because of the model's complexity, which imply a large number of parameters and in consequence a large sample set for the SA, Duarte [26] first used Morris method to reduce the number of parameters. The limitation in this method, however, is that Morris does not provide a quantitative indication of the exact differences in influence between parameters.

FAST [24] is a quantitative method that estimates the fractional contribution of each input factor to the variance of the output. This method calculates only the first order effects, or in the case of the Extended FAST, the first order and the total order effects on output variance. The Sobol method [13] is another approach based on variance estimation techniques. This method extends beyond the FAST approach, allowing the estimation of the first order, N order, and total order effects. As such, because it is the most comprehensive approach, the Sobol method is used in this study. A more detailed description of the Sobol method is provided in Chapter 5.

## 2.4 Parallel Computing

Working with large data sets, in addition to having numerous parameters and equations, implies an increase in the runtime required for model execution and analysis. This situation often limits investigators in their studies because of a lack of computational power to fully perform their analysis. We use high performance computing to overcome these limitations in the sensitivity analysis.

Parallel computing is essentially the execution of numerous tasks simultaneously over multiple processors. The execution of tasks requires the elaboration of a parallel program to allow the partition and processing of the data on multiple processors. Generally, a set of processors perform the same task over different portions of data.

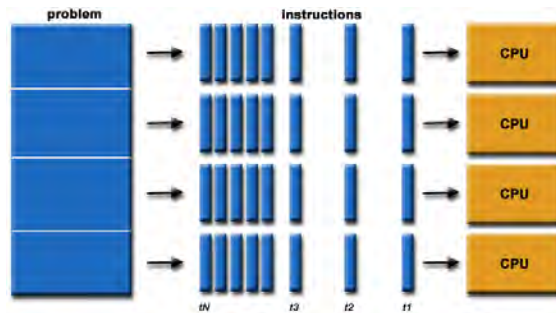


Figure 2.5: Scheme of a parallel problem [6]

There are a many different architectures used in parallel computing, as well as parallel programming models. Principal architectures and parallel programming models are presented in the following sections.

#### 2.4.1 Parallel architectures

- *Shared Memory*

In this architecture, all processors share the same memory and consequently there is a global address space. The actions on the memory by one processor are seen by all other processors, and as the number of processors increases, there is more difficulty accessing the memory. Shared memory architectures are divided into two classes depending on the memory access time, uniform memory access (UMA) and non-uniform memory access (NUMA). For UMA, there is equal access time to all parts of memory. This can also be called cache coherent UMA (CC-UMA), where any change in a location of shared memory is seen by all the processors. For NUMA, access time to the memory is not equal, which can be slow. As with UMA and CC-UMA, there is also cache coherent NUMA (CC-NUMA).

- *Distributed Memory*

In this architecture, each processor has its own memory and there is a network to interconnect individual processor memory space (but there is not a global

address space). Additionally, each processor can rapidly access its own memory without interference from other processors. This is referred to as memory scalable, where a larger number of processors means larger memory. However, communication between processors and synchronizing between tasks is the explicit responsibility of the programmer.

A number of approaches exist to deal with both distributed and shared memory access. In this work the solution of the SAI model is implemented on a distributed memory architecture using the Message Passing Interface MPI [18] as described below.

#### 2.4.2 Message Passing Interface (MPI)

MPI is a standard library that allows the communication of multiple processes in a distributed memory environment [18]. The transfer of data is handled by cooperative operations, which have to be matched. MPI programs can be used and compiled on a wide variety of parallel computers, such as the IBM SP2, the Silicon Graphics Origin 2000, or on a cluster of workstations (homogenous or heterogeneous) over a network. There are also different versions of MPI implementations (e.g. MPICH [27] and LAM-MPI [19]).

- *MPICH*: MPI/Chameleon has two versions<sup>2</sup>, MPICH1 (MPI 1.1) and MPICH2 (MPI 2.0). MPICH2 essentially replaces MPICH1 and works on different platforms, such as clusters and SMPs (Symmetric Multiprocessor machines). MPICH2 works on several operating systems, including Linux, Mac OS/X, Solaris and Windows.

---

<sup>2</sup> <http://www-unix.mcs.anl.gov/mpi/mpich/index.htm>

- *LAM-MPI*: Local Area Multicomputer-MPI [19] was developed for use in heterogeneous clusters and on SMPs machines. The principal objects in this approach are the nodes (physical computers), the processes (programs) and the messages (data transmitted). To coordinate the interaction of these objects, LAM-MPI uses an identification number, specifically the node ID. The node ID is then used to execute the different processes without loss or conflict.

The parallel implementation in this work used LAM-MPI 7.1.1 running on a Linux cluster, but because of its portability, the same code can be easily executed on other parallel systems.

## CHAPTER 3

# SEMI-ANALYTICAL INVERSION MODEL

This chapter presents the mathematical foundation of the SAI model for shallow waters is presented. The parameters of interest and nuisance parameters that are used in the model and examined using the sensitivity analysis are also defined.

### 3.1 Mathematical Foundation of the SAI model

The SAI model is an approximation of the radiative transfer equation for simulating the interaction of EMR within shallow water. As described in Chapter 2, the interaction process of EMR changes as a function of several factors, particularly absorption and scattering, which are both inherent optical properties. The Lee et al. model [1], [2] was developed to retrieve shallow water bathymetry, bottom albedo and water properties from hyperspectral imagery. The parameters of interest retrieved from the model are: P, G, BP, B, and H (see the parameters definition in Table 3.1).

Table 3.1: Definition of parameters, [1], [2]

Parameter	Definition	Units
$a$	Absorption coefficient of the total	$m^{-1}$
$a_w$	Absorption coefficient of pure seawater	$m^{-1}$
$a_\phi$	Absorption coefficient of phytoplankton pigments	$m^{-1}$
$a_g$	Absorption coefficient of gelbstoff	$m^{-1}$
$a_o, a_1$	Empirically derived coefficients	
$b_b$	Backscattering coefficient of the total	$m^{-1}$
$b_{bw}$	Backscattering coefficient of seawater	$m^{-1}$
$b_{bp}$	Backscattering coefficient of particles and viewing-angle	$m^{-1}$
B	Bottom reflectance at 550 nm	
BP	Combined influences from particle backscattering coefficient, view angle and sea state	$m^{-1}$
$D_u^B$	Distribution function for scattered photons from the bottom	
$D_u^C$	Distribution function for scattered photons from the water	
$\Delta$	Spectrally constant offset	
G	Absorption coefficient gelbstoff and detritus at 440 nm	$m^{-1}$
H	Water depth	m
$\kappa$	Diffuse attenuation coefficients	$m^{-1}$
$\lambda$	Wavelength	nm
$\rho$	Bottom reflectance, albedo	
$\rho_{sd}$	Sand albedo (reflectance) at 550 nm	
P	Phytoplankton absorption coefficient at 440 nm	$m^{-1}$
$r_{rs}$	Subsurface remote sensing reflectance	$sr^{-1}$
$r_{rs}^{dp}$	Subsurface remote sensing reflectance for optically deep water	$sr^{-1}$
$R_{rs}$	Above-surface remote sensing reflectance	$sr^{-1}$
$\hat{R}_{rs}$	Estimated of Above-surface remote sensing reflectance	$sr^{-1}$
$\theta_w$	Subsurface solar zenith angle	rad
u	Ratio of backscattering coefficient to the attenuation coefficient	
Y	Spectral power for particle backscattering coefficient	

The inversion approach for implementing this model utilizes a predictor-corrector scheme to optimize values for the parameters of interest, while minimizing the error function (objective function). The objective function is defined as:

$$err = \frac{\left[ \sum_{405}^{675} \left( R_{rs}(\lambda) - \hat{R}_{rs}(\lambda) \right)^2 + \sum_{720}^{800} \left( R_{rs}(\lambda) - \hat{R}_{rs}(\lambda) \right)^2 \right]^{0.5}}{\left[ \sum_{405}^{675} \left( \hat{R}_{rs}(\lambda) \right)^2 + \sum_{720}^{800} \left( \hat{R}_{rs}(\lambda) \right)^2 \right]^{0.5}} \quad (3.1)$$

where  $\hat{R}_{rs}(\lambda)$ , an apparent optical property, is the relation between the water leaving radiance to downwelling irradiance. The cutoff between 675 nm and 720 nm is caused by the absence of variables in the model that express the solar-simulated chlorophyll [28] fluorescence, which is an absorption feature around of 680 nm. The range of 720 nm to 800 nm is significant in case of turbid water. This objective function is essentially the root square error between modeled,  $\hat{R}_{rs}(\lambda)$ , and measured  $R_{rs}(\lambda)$ , surface remote sensing reflectance. The modeled reflectance is calculated with the SAI model and the measured is from a hyperspectral image. The objective function used in this study (Equation 3.1) was previously implemented by Goodman [5] as a slightly modified version of the function utilized by Lee et al [2], [28].

The following equations define the model derivation of  $\hat{R}_{rs}(\lambda)$ . The surface reflectance is a function of the subsurface remote sensing reflectance,  $r_{rs}(\lambda)$ , the ratio of the upwelling radiance to the downwelling irradiance just below the water surface, as defined using Equation 3.2:

$$\hat{R}_{rs}(\lambda) = \frac{0.5 r_{rs}(\lambda)}{1 - 1.5 r_{rs}(\lambda)}. \quad (3.2)$$

The quantity  $r_{rs}$  is in turn defined as the sum of contributions from the water column  $r_{rs}^C(\lambda)$  and bottom,  $r_{rs}^B(\lambda)$  as previously described in Equation 2.3:

$$r_{rs}(\lambda) = r_{rs}^C(\lambda) + r_{rs}^B(\lambda), \quad (3.3)$$

The portion of the equation representing the water column,  $r_{rs}^C(\lambda)$ , is defined as:

$$r_{rs}^C(\lambda) = r_{rs}^{dp}(\lambda) \left[ 1 - \exp \left( - \left[ D_u^C(\lambda) + \frac{1}{\cos \theta_w} \right] \kappa(\lambda) H \right) \right], \quad (3.4)$$

where  $1/\cos(\theta_w)$ , also known as  $D_o$ , represents a non-lambertian field, which means path length can increase with larger viewing angles, and will also vary with the radiance distribution incident on the sea surface [29]. The solar zenith angle  $\theta_w$  is a function of solar position at the time the hyperspectral imagery was acquired. In this study,  $\theta_w$  is  $9^\circ$ , which is the value used by Goodman [5], in his analysis of Kaneohe Bay. However, this value typically varies from  $0^\circ$  to  $45^\circ$ . Additionally, the values for water depth,  $H$ , are limited so as not to exceed 30 meters.

The subsurface remote sensing reflectance for optically deep water,  $r_{rs}^{dp}(\lambda)$ , is defined by:

$$r_{rs}^{dp}(\lambda) \approx (0.084 + 0.17u(\lambda))u(\lambda), \quad (3.5)$$

and the distribution function for the water column,  $D_u^C(\lambda)$ , which indicates the attenuation of the upwelling EMR in the water column, is defined as:

$$D_u^C(\lambda) \approx 1.03(1 + 2.4u(\lambda))^{0.5}. \quad (3.6)$$

The second portion of equation for  $r_{rs}(\lambda)$ , the contribution from the bottom  $r_{rs}^B(\lambda)$ , is defined as:

$$r_{rs}^B(\lambda) = \frac{1}{\pi} \rho(\lambda) \exp \left( - \left[ D_u^B(\lambda) + \frac{1}{\cos \theta_w} \right] \kappa(\lambda) H \right). \quad (3.7)$$

The contributions from the bottom reflectance,  $\rho(\lambda)$ , which includes one of the parameters of interest, is defined by:

$$\rho(\lambda) = B\rho_{sd}(\lambda), \quad (3.8)$$

where  $\rho_{sd}(\lambda)$ , is the bottom reflectance of sand normalized to 1.0 at 550 nm and  $B$  is the albedo a 550 nm. In other words, the bottom is considered only sand but the albedo intensity can change from place to place as a function of  $B$ .

The attenuation function from the bottom,  $D_u^B(\lambda)$ , which indicates the attenuation of upwelling EMR from the bottom, is defined as:

$$D_u^B(\lambda) \approx 1.04(1 + 5.4u(\lambda))^{0.5}. \quad (3.9)$$

The terms  $u(\lambda)$  and  $\kappa(\lambda)$ , which are found in Equations 3.4, 3.5, 3.6, 3.7, and 3.9, are functions of the inherent optical properties. They are defined as:

$$u(\lambda) = b_b(\lambda)/\kappa(\lambda), \text{ and} \quad (3.10)$$

$$\kappa(\lambda) = a(\lambda) + b_b(\lambda), \quad (3.11)$$

where  $a(\lambda)$  is the absorption coefficient and  $b_b(\lambda)$  is the backscattering coefficient. The absorption coefficient,  $a(\lambda)$ , is defined as the sum of the absorption coefficient of pure water,  $a_w(\lambda)$ , the absorption coefficient of phytoplankton,  $a_\phi(\lambda)$ , and the absorption coefficient of gelbstoff,  $a_g(\lambda)$ . Thus,

$$a(\lambda) = a_w(\lambda) + a_\phi(\lambda) + a_g(\lambda), \quad (3.12)$$

where  $a_\phi(\lambda)$  is defined as:

$$a_\phi(\lambda) = [a_o(\lambda) + a_1(\lambda)\ln(P)]P, \quad (3.13)$$

and values for  $a_w(\lambda)$ , which is a physical property, and  $a_o(\lambda)$  and  $a_1(\lambda)$ , which are empirical spectra derived by Lee et al., are presented in Table 3.2.

The parameter  $P$  is the phytoplankton absorption coefficient at 440 nm,  $a_\phi(440)$ . Lee et al. [1] found that  $P$  varies as a function of the chlorophyll a concentration,

Table 3.2: Spectral data for absorption parameters

$\lambda$	$a_o$	$a_1$	$a_w$	$\lambda$	$a_o$	$a_1$	$a_w$
403.77	0.7177	0.0144	0.0051	606.85	0.2596	0.0544	0.2599
413.43	0.8065	0.0100	0.0047	616.53	0.3057	0.0645	0.2702
423.09	0.8951	0.0051	0.0047	626.21	0.3344	0.0702	0.2855
432.75	0.9674	0.0013	0.0054	635.90	0.3412	0.0709	0.3031
442.42	0.9858	0.0020	0.0071	645.58	0.3331	0.0678	0.3274
452.08	0.9577	0.0069	0.0090	655.02	0.4349	0.0887	0.3723
461.75	0.9180	0.0119	0.0100	664.89	0.7173	0.1396	0.4274
471.41	0.8564	0.0148	0.0110	674.43	0.8379	0.1555	0.4471
481.08	0.7918	0.0179	0.0129	683.97	0.6129	0.1170	0.4838
490.75	0.7549	0.0304	0.0158	693.52	0.3011	0.0607	0.5501
500.41	0.7289	0.0569	0.0218	703.07	0.1182	0.0237	0.6806
510.08	0.6884	0.0839	0.0320	712.62	0.0494	0.0099	0.9273
519.76	0.6331	0.0963	0.0407	722.17	0.0228	0.0048	1.3389
529.43	0.5724	0.0967	0.0433	731.73	0.0130	0.0028	1.8026
539.10	0.5089	0.0901	0.0476	741.29	0.0130	0.0028	2.3953
548.78	0.4359	0.0795	0.0545	750.86	0.0130	0.0028	2.4733
558.45	0.3584	0.0681	0.0614	760.42	0.0130	0.0028	2.5021
568.13	0.3043	0.0610	0.0682	770.00	0.0130	0.0028	2.4700
577.81	0.2806	0.0581	0.0858	779.57	0.0130	0.0028	2.3615
587.49	0.2657	0.0555	0.1242	789.15	0.0130	0.0028	2.1978
597.17	0.2448	0.0507	0.1881	798.72	0.0130	0.0028	1.9924

[chl-a]. Thus, if measurements were available, the value for P could be directly input to the model, but in most cases it is typically derived as one of the parameters of interest.

The absorption coefficient of gelbstoff,  $a_g(\lambda)$ , is approximated by:

$$a_g(\lambda) = G \exp[-S(\lambda - 440)]. \quad (3.14)$$

where G is the absorption coefficient of gelbstoff and detritus at 440 nm. Gelbstoff, also known as yellow substance or colored dissolved organic matter (CDOM), is a mix of humic and fulvic acids, which are compounds of dissolved and colloidal organics. Detritus is organic material suspended in water, and along with gelbstoff, has an important contribution to the total absorption coefficient in the visible wavelengths.

Bricaud [30] originally developed Equation 3.14 for the range from 375 - 500 nm, and Lee et al. extended the range to 800 nm. The parameter  $S$  defines the spectral slope of  $a_g(\lambda)$  and is discussed in further detail in the next section.

The backscattering coefficient  $b_b(\lambda)$  is the sum of the backscattering coefficient of seawater,  $b_{bw}(\lambda)$ , and the backscattering coefficient of particles,  $b_{bp}(\lambda)$ :

$$b_b(\lambda) = b_{bw}(\lambda) + b_{bp}(\lambda), \quad (3.15)$$

$$b_{bw}(\lambda) = 0.0038(400/\lambda)^{4.3}, \quad (3.16)$$

$$b_{bp}(\lambda) = BP(400/\lambda)^Y. \quad (3.17)$$

Equation 3.17 describes the backscattering by particles, where  $BP$  is a combination of particle backscattering coefficient, view angle and sea state. Gordon et al. [29] assume a value of 0.01 for  $BP$  with excellent agreement between real and computed data. However, here it derived as one of the parameters of interest. Although these data were determined for Case 1 waters, which depend on [chl-a], it can be extended to Case 2 waters with variations in concentrations of other elements such as gelbstoff, suspended particles and influence from the bottom.

In summary, the five parameters of interest are  $P$ ,  $G$ ,  $BP$ ,  $B$  and  $H$ , which are derived using an inversion modeling approach. Other parameters in the model are considered nuisance parameters.

### 3.1.1 Nuisance Parameters

Nuisance parameters are an important aspect of the model for deriving the parameters of interest. In this model, the values for most of the nuisance parameters were determined empirically using field data and observations from Hydrolight [1],

[2]. It is important to know the relative influence of these parameters over a given range of acceptable values in order to examine their impact on the parameters of interest. A sensitivity analysis is utilized to investigate their influence. The nuisance parameters included in this analysis are presented below.

### 3.1.1.1 Spectral slope of $a_g$ (S)

The spectral slope of  $a_g$ , S in Equation 3.14, is a proxy for variations in the composition of gelbstoff. The greatest gelbstoff concentrations are found typically in lakes, rivers and coastal water [22], and the dominant absorption for gelbstoff is in the blue region of the spectrum. Lee et al. [2] indicates that S influences both P and G, and has a smaller influence on H, which has more dependency from the total absorption. A study by Twardowski et al. [31] collected values of S presented by different authors, and concluded that a typical value was between 0.014-0.015  $nm^{-1}$  ([30], [2]), but that in some instances the values could be much higher (e.g., 0.023  $nm^{-1}$ ). Lee et al. [1], [2] and Goodman [5], use a value of 0.015  $nm^{-1}$  for S, which represents an average for the range from 0.011-0.021  $nm^{-1}$  [32]. For this study, the later range is used.

### 3.1.1.2 Spectral shape parameter (Y)

The parameter Y, in Equation 3.17, is the wavelength power of  $b_{bp}$  and varies as a function of particle size and chlorophyll, sediment and gelbstoff concentration. There are no direct measurements of Y and its value is assumed dependent on [chl-a], where Y is large for large values of [chl-a]. A suggested range is 0-3 [28], but as used by Lee et al. [1] and Goodman [5] in the SAI model, it is limited to the range from 0-2.5. This range is comparable with the range suggested by Liew [33], where not only [chl-a] is taken into account, but also the concentration of gelbstoff and suspended particles. Liew defines two cases: Y=0, which has an average [chl-a] and

high concentration of suspended sediments with fine particles; and  $Y=2.2$ , which has low [chl-a] and low suspended sediments with large particles. Lee et al. [2] showed that smaller  $Y$  values produce smaller values of  $G$  and larger  $Y$  values produce larger values of  $G$ . An empirical relationship can be used for determining  $Y$ :

$$Y \approx 3.44[1 - 3.17\exp(-2.01R_{rs}(440)/R_{rs}(490))]. \quad (3.18)$$

However, this equation is not used in the current study. Instead, the range of values from 0-2.5 are used in the sensitivity analysis to investigate the influence.

### 3.1.1.3 Constants of $b_{bw}$

There are two constants in Equation 3.16: 0.0038 (np5) and 4.3 (np6). Lee et al. [2] derived the values for these parameters from Smith and Baker [34]. Although this work was completed some years ago, the values are still valid and utilized in many different investigations (e.g. [2], [35]). The range of variability for np5 and np6 used in the sensitivity analysis are +25% and -5%, as suggested by Smith and Baker [34], which results in a range of 0.0036-0.00475 for np5 and 3.87-4.73 for np6.

### 3.1.1.4 Constants of $D_u^C$

The constants in Equation 3.6, 1.03 ( $D_o$ ) and 2.4 ( $D_1$ ) were empirically derived by Lee et al. [1] using Hydrolight simulations. Results from this analysis indicated agreement of  $\pm 3\%$  for different values of  $u$ . It was also determined that these constants can influence  $H$ , one of the parameters of interest. Lee et al. suggest a range of 1.2-1.7 for  $D_u^C$ , but does not indicate individual ranges for  $D_o$  and  $D_1$ . Thus, the range of values used for  $D_o$  and  $D_1$ , based on  $\pm 10\%$  from the derived values of 1.03 and 2.4, which equates to 0.927-1.133 and 2.16-2.64, respectively.

### 3.1.1.5 Constants of $D_u^B$

As with  $D_u^C$ ,  $D_u^B$ , Equation 3.9 also contains empirically derived constants, 1.04 ( $D_{op}$ ) and 5.4 ( $D_{1p}$ ), which can also influence model output. Lee et al. indicate a range of 1.1-2.2 for  $D_u^B$ , with no indication regarding the individual constants. Thus, again using  $\pm 10\%$ , the ranges used for  $D_{op}$  and  $D_{1p}$  are 0.936-1.144 and 4.86-5.94, respectively.

### 3.1.1.6 $g_o$ and $g_1$

These parameters  $g_o$  and  $g_1$  relate  $r_{rs}^{dp}$  with the absorption and backscattering coefficients, and thus can influence G and BP. Equation 3.5 was developed for Case I waters [29], but it has also been found to work for other water type as well. Lee et al. [1] selected values for the parameters by optimizing the fit between simulated SAI model output and simulated data from Hydrolight. The final values used in Equation 3.5 are 0.084 for  $g_o$  and 0.17 for  $g_1$ . Based on  $\pm 10\%$  of these values, the range used in the sensitivity analysis are 0.0756-0.0924 for  $g_o$  and 0.153-0.187 for  $g_1$ .

### 3.1.1.7 $\zeta$ and $\Gamma$

The parameters  $\zeta = 0.5$  and  $\Gamma = 1.5$  in Equation 3.2 relate above surface to below surface remote sensing reflectance. The values for  $\zeta$  is defined by:

$$\zeta = \frac{t_- t_+}{n^2}, \quad (3.19)$$

where  $t_-$  is the radiance transmittance,  $t_+$  is the irradiance transmittance, which define the transfer of EMR from below to above the surface, and  $n$  is the refractive index of water. Gordon [29] defines  $\Gamma$  as the water-air reflectance for totally diffuse irradiance. This parameter is part of the denominator of Equation 3.2 ( $1 - \Gamma r_{rs}$ ), which represents the internal reflection from water to air. In open-ocean waters,

internal reflections are typically insignificant but for shallow or turbid waters can be substantial. The values employed by Lee et al. [1],[2] are consistent with values calculated using Hydrolight ( $\zeta \approx 0.518$ ,  $\Gamma \approx 1.562$ ), and with values reported by Gordon [29] ( $\zeta \approx 0.48$ ). Using  $\pm 10\%$ , the ranges used in the sensitivity analysis are 0.45 - 0.55 for  $\zeta$  and 1.35 - 1.65 for  $\Gamma$ .

### 3.2 Synthetic data for experiments

As mentioned before, an inversion routine is used to retrieve the five parameters of interest in the SAI model. For the sensitivity analysis, this process is repeated numerous times using different values for the input parameters. For this study, the model used a total of 42 bands from 400-800 nm, each with a spectral resolution of approximately 10 nm. Two different synthetic vectors were used to analyze model performance and implement the sensitivity analysis, one for clear water (minimal influence from water constituents) and one for optically dense water (significant influence from water constituents). These vectors were created by applying the SAI model in a forward approach, using the parameters of interest as input and obtaining surface reflectance as output. This was performed using two different sets of input parameters for P, G, BP, and B, as well as six different values for H (see Table 3.3), resulting in a total of 12 vectors. By using these synthetic vectors rather than real data, results of the inversion can be directly compared with the actual parameters of interest used to create the synthetic data.

Table 3.3: Initial values for clear and optically dense water and range of parameters of interest

	<b>P</b>	<b>G</b>	<b>BP</b>	<b>B</b>	<b>H</b>
Clear Water	0.05	0.05	0.01	0.4	1,5,10,15,20,30
Optically Dense Water	0.4	1	0.2	0.4	1,5,10,15,20,30
Range	0.005-0.5	0.002-3.5	0.001-0.5	0.01-0.6	0.2-33

This chapter described the SAI model and specified the values and ranges for the parameters of interest and nuisance parameters used in the model and in the sensitivity analysis tests. Chapter 4 explains how the parallel implementation was done, what results in terms of time were obtained, what optimization was used to perform the inversion model, and details of the Sobol method used to implement the sensitivity analysis. Results from the two types of synthetic vectors, for clear water and optically dense water are presented in Chapter 5.

# CHAPTER 4

## PARALLEL IMPLEMENTATION OF SAI MODEL AND EXPERIMENTAL RESULTS

This chapter discusses the implementation of the semi-analytical inversion model within a parallel processing framework. The greater processing speed obtained with this parallel implementation is also demonstrated. This approach provides the foundation for assessing real-time processing capabilities as well as the computation power necessary for addressing complex optimization and sensitivity questions. Details of implementing the optimization routine using GENCAN method are described. Finally performance results for SAI model parallel implementation are shown.

### 4.1 Implementation of SAI model within a Parallel Processing Framework

The semi-analytical inversion model was implemented withing a parallel processing framework using C++ and LAM-MPI [18]. As discussed in Chapter 3, MPI is the de facto standard for implementing parallel applications on distributed memory systems. The specific version used in this research is LAM-MPI 7.1.1. The Parallel and Distributed Computing Laboratory (PDCLab) at the University of Puerto Rico at Mayaguez (<http://pdc.ece.uprm.edu>) facilitated use of an IBM 64 dual-processor nodes xSeries Server cluster running under Linux.

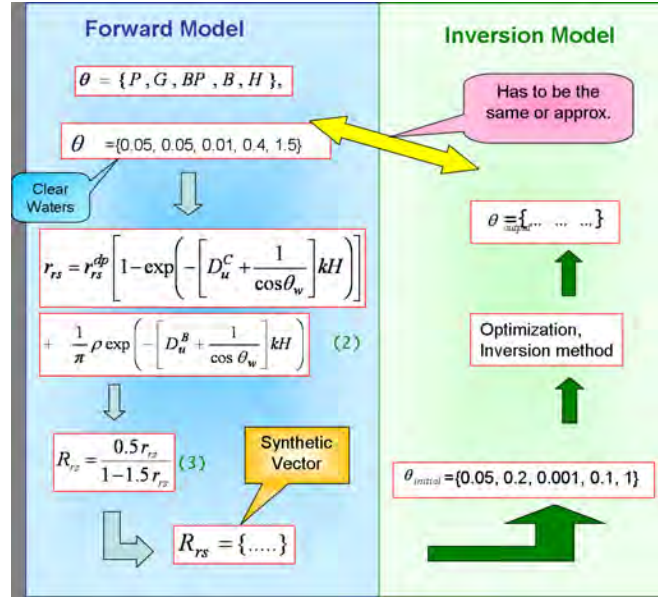


Figure 4.1: Implementation of the semi-analytical model as a forward and inverse model

Figure 4.1 presents the two-part scheme of the SAI model. The first part of the overall scheme is the forward implementation, where the semi-analytical model is utilized to create a set of synthetic vectors  $\hat{R}_{rs}$  (equivalent to the individual pixel of a hyperstectral image). These synthetic pixels were created using the two types of parameters of interest values: one for clear waters and one for optically dense waters (Table 3.3). The second part of the overall scheme is the inversion model, where the optimization method is utilized to retrieve the values for the parameters of interest for each of the synthetic vectors using varying combinations of nuisance parameters. This second part represents the portion that would be applied to a hyperspectral image, using one set of nuisance parameters to retrieve the water optical properties, bottom albedo and bathymetry. However, in order to more thoroughly analyze model performance, synthetic vectors are utilized so that the exact values of the parameters of interest are known. The sensitivity analysis (SA) operates on the complete result matrix of parameters of interest for each of the synthetic vectors,

and is ultimately used to examine the influence of the nuisance parameters on the parameters of interest.

The overall problem addressed by the parallel implementation can be described as a simple decomposition into independent parts that can be processed simultaneously, with communication of processors (slaves) and master processor occurring only at the start and end of the application. This decomposition permits the master to send one array of nuisance parameters to every processor for its implementation in the optimization routine. This is possible because the implementation of the nuisance parameters is independent on each other. Therefore, the processing is achieved using a master-slave scheme [36] such that the master coordinates all the processes and slaves are in charge of the actual vector creation and optimization for each set of nuisance parameters.

## 4.2 Non-linear constrained optimization

As mentioned before, the focus of the study is to examine the SAI model with respect to evaluating the impact of the nuisance parameters on model performance. The foundation of the SAI model is the optimization routine employed for retrieving estimates of bathymetry and water properties. The goal of the optimization routine is to identify the best value for the parameters of interest that minimize a given objective function. The objective function used for performing this optimization (as presented in Chapter 3) is defined as:

$$err(\theta, \gamma) = \frac{|R_{rs} - \hat{R}_{rs}(\theta, \gamma)|_2^2}{|\hat{R}_{rs}(\theta, \gamma)|_2^2}, \quad (4.1)$$

where  $err(\theta, \gamma)$ , which is evaluated from 405-675 nm and 720-800 nm, is a function of the variables or parameters of interest ( $\theta$ ):

$$\theta = \{P, G, BP, B, H\},$$

and the nuisance parameters  $\gamma$ :

$$\gamma = \{S, Y, np5, np6, D_o, D_1, D_{op}, D_{1p}, g_o, g_1, \zeta, \Gamma\}.$$

The SAI model is non-linear and the parameters of interest are constrained within bounds representing reasonable physical limits. Consequently, the solution is a non-linear constrained optimization.

The non-linear constrained optimization problem is solved using the GENCAN routines from the OOL (Open Optimization Library). OOL [37] is implemented following the GNU Scientific Library (GSL) standards and operates under the General Public License (GPL). OOL also utilizes a different set of notation when referring to the objective function and related parameters. In this notation, the objective function  $err(\theta, \gamma)$  is represented by  $f(x)$ , the parameters of interest  $\theta$  is represented by  $x$ , and the nuisance parameters  $\gamma$  are not directly expressed. The optimization problem is expressed as [38]:

$$\text{Minimize } f(x) \text{ subject to } x \in \Omega, \quad (4.2)$$

where  $l$  is the lower bound,  $u$  is the upper bound and  $\Omega$  is the closed convex set (box set) in  $\mathfrak{R}^n$ , defined as:

$$\Omega = \{x \in \mathfrak{R}^n \mid l \leq x \leq u\}. \quad (4.3)$$

and  $\Omega$  is divided into disjoint open faces  $F_I$ , for all  $I \subset \{1, 2, \dots, n, n+1, n+2, \dots, 2n\}$ , such that:

$$F_I = \{x \in \Omega \mid x_i = l_i \text{ if } i \in I, x_i = u_i \text{ if } n+i \in I, l_i < x_i < u_i \text{ otherwise}\}. \quad (4.4)$$

GENCAN incorporates two different methods for minimizing a given objective function, the truncated Newton method, and the Spectral Projected Gradient (SPG)

method. To determine which method is utilized GENCAN executes the test:

$$\|g_I(x_k)\| \geq \eta \|g_P(x_k)\|, \quad (4.5)$$

where  $\eta \in (0, 1)$ ,  $x_k \in \Omega$  (i.e., inside a given face of  $\Omega$ ), and  $g_P(x)$  is the projected gradient defined as:

$$g_P(x) = P_\Omega(x - g(x)) - x, \quad (4.6)$$

where  $g_x$  denotes  $\nabla f_x$  and  $g_I(x)$  is the projection of  $g_P(x)$  inside the face  $S_I$ . For all  $x \in F_I$ ,  $g_I(x)$  is defined as

$$g_I(x) = P_{S_I}[g_P(x)], \quad (4.7)$$

where  $S \subset \mathfrak{R}^n$ , which is the parallel linear subspace to  $V_I$ , the smallest affine subspace that contains  $F_I$ .

If the test in Equation 4.5 is true, the truncated Newton method is performed to compute  $x_{k+1}$ . If not, it is necessary to leave the current face and the new iteration is computed with the non-monotone SPG method.

If selected, the Truncated Newton method, also known as Line Search Newton - Conjugate Gradient (CG) method, is used to compute the search direction  $d_k$  to calculate the iteration  $x_{k+1}$ , defined as:

$$x_{k+1} = x_k + \alpha_k d_k, \quad (4.8)$$

where  $\alpha_k$  is the step length and the maximum  $\alpha_{max} = 1$ . The search direction is computed by applying CG method to the Newton Equation:

$$Ad_k = -g(x_k), \quad (4.9)$$

where the Hessian  $A = \nabla^2 f(x_k)$  and  $g(x_k) = \nabla f(x_k)$ . In this approach, GENCAN does not need explicit knowledge of the gradient and Hessian. The gradient is calculated using finite differences given by:

$$g(x_k) = \frac{f(x_k + \varepsilon e_i) - f(x_k - \varepsilon e_i)}{2\varepsilon} + O(\varepsilon^2), \quad (4.10)$$

where  $e_k$  is the  $k$ -th unit vector, and  $\varepsilon$  is a small perturbation of  $x$ . GENCAN requires the product of  $A$   $d_k$ , where instead of computing just the Hessian, the product of matrix-vector is calculated as:

$$Ad_k = \left( \frac{g(x_k + \varepsilon e_i) - f(x_k - \varepsilon e_i)}{2\varepsilon} \right)^T d_k. \quad (4.11)$$

The line search ends if  $x_k + d_k$  satisfies the sufficient descent criterion  $f(x_k + \alpha_{max}d_k) < f(x_k)$  and if the directional derivative  $\langle g(x_k + d_k), d_k \rangle$  is substantially larger than  $\langle g(x_k), d_k \rangle$ . When the directional derivative is not sufficiently large, larger step values are needed to obtain smaller functional values. Then,  $\alpha$  is multiplied by a fixed factor  $N$ , a process is called extrapolation. In the other case, when the sufficient descent criterion is not satisfied, backtracking is performed, which means the Armijo condition has to be satisfied:

$$f(x_k + \alpha d_k) \leq f(x_k) + \gamma \alpha \langle g_k, d_k \rangle. \quad (4.12)$$

Further detail regarding the Truncated Newton method is provided in [38].

Where the Truncated Newton method is not used, the SPG method is used instead. The SPG method is a modification of the Barzilai-Borwein gradient method presented by Birgin et al [39]. In this method, the search direction  $d_k$  is define as:

$$d_k = P_\Omega(x_k - \lambda_k g(x_k)) - x_k, \quad (4.13)$$

where  $\lambda = 1/\alpha_k$  and  $x_{k+1} = x_k + \lambda d_k$  is computed until the Armijo condition (Equation 4.12) is fulfilled. The parameter  $\alpha_k$  is defined by:

$$\alpha_k = \frac{s_{k-1}^T Y_{k-1}}{s_{k-1}^T s_{k-1}}, \quad (4.14)$$

and has the following range of value:

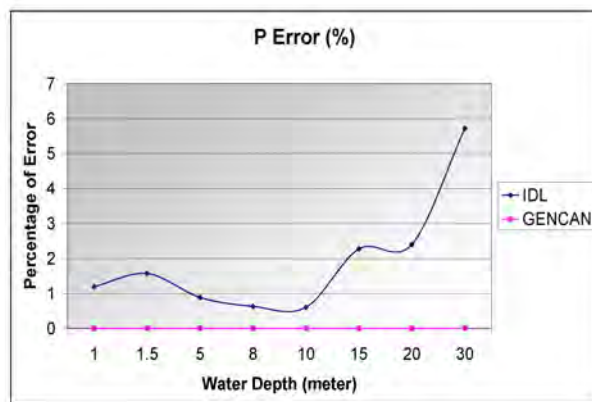
$$\alpha_k = \min \{ \alpha_{max}, \max \{ \alpha_{min}, \alpha_k^T \} \}. \quad (4.15)$$

where the slack variables  $s_k = x_{k+1} - x_k$  and  $Y_k = g(x_{k+1} - g(x_k))$  are used to estimate  $\alpha_k$ , which can only assume positive values.

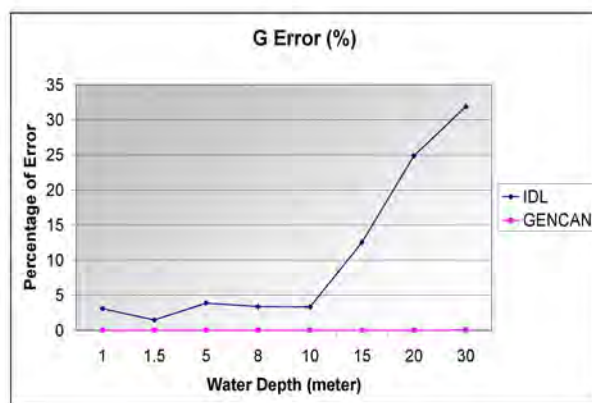
### 4.3 Results of Optimization Routine Test

The accuracy of the GENCAN optimization routine has been verified using two synthetic pixels with characteristics of clear water and optically dense water at eight different water depths. The values used to create the pixel were  $P=0.05$ ,  $G=0.05$ ,  $BP=0.001$ ,  $B=0.4$ , for clear water, and  $P=0.4$ ,  $G=1$ ,  $BP=0.2$ ,  $B=0.4$ , for optically dense water and  $H$  was tested with : 1, 1.5, 5, 8, 10, 15, 20, 30 meters. Because the synthetic pixels are generated using a forward version of the SAI model, optimization results should obtain the same values for the parameters of interest as were used as input. Results of GENCAN routine are also compared with an IDL optimization routine. Figure 4.2, 4.3 and 4.4 show the percentage of error obtained for each parameter of interest in case of clear water after optimization with GENCAN and IDL. In general GENCAN yields percentages of errors under 1%, except for parameters  $B$  and  $H$  at 30 meters of depth. In this case the percentages of error were 23.12% and 4.91%, respectively.

When comparing the results to the IDL optimization for clear water significant differences in terms of the percentage of error can be appreciated. For instance, the error for the parameter  $G$  is 30% with IDL optimization compared to 0% of error with GENCAN optimization (see Figure 4.2(b)).

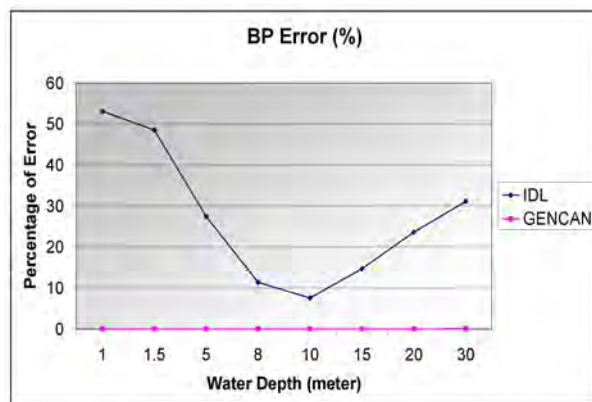


(a)

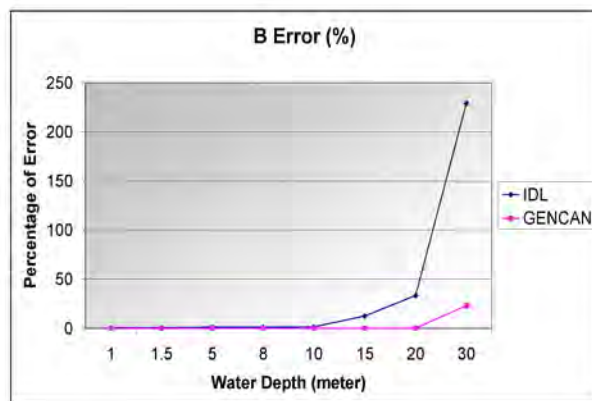


(b)

Figure 4.2: Percent Errors for IDL and GENCAN optimization methods for clear water



(a)



(b)

Figure 4.3: Percent Errors for IDL and GENCAN optimization methods for clear water, continuation

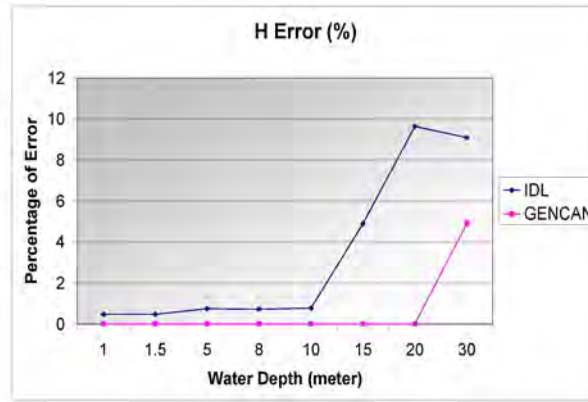
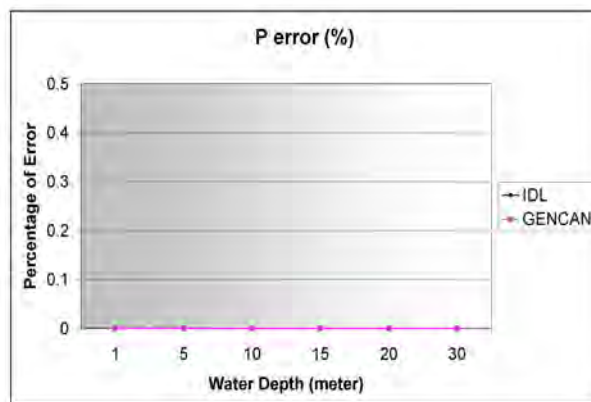
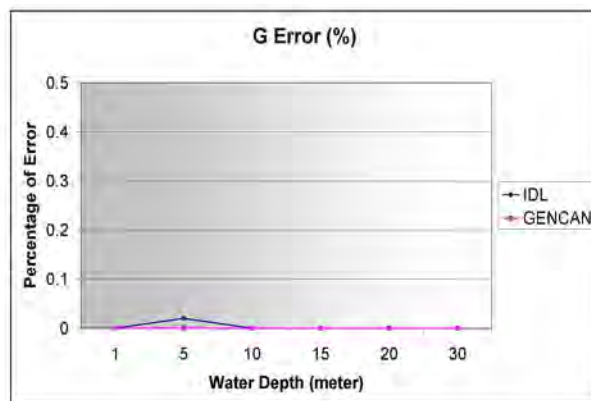


Figure 4.4: Percent Errors for IDL and GENCAN optimization methods for clear water, continuation

The test done with a synthetic pixel for optically dense water are illustrated in Figure 4.5, 4.6 and 4.7, illustrate good results for parameters P, G and BP where the error is almost zero for both GENCAN and IDL optimization. However, for parameters B and H the percentage of error increase with water depth. For parameter B, GENCAN shows an error of 33.33% from 10 meters to 30 meters, and IDL shows an error of 33.33% from 5 meters to 30 meters. For parameter H, GENCAN presents an error of 68.29% at 10 meters and this error increase until get an error of 409.81% at 30 meter, and IDL also presents an increasing error beginning from 5 meters with 22.44% until get 409.81% at 30 meters. These results demonstrate the difficulty of the extraction of information for bottom albedo and water depth with optically dense water, where at larger water depth larger decreasing on light when it is traveling through the water column and consequently there is not enough light to be reflected from the surface.

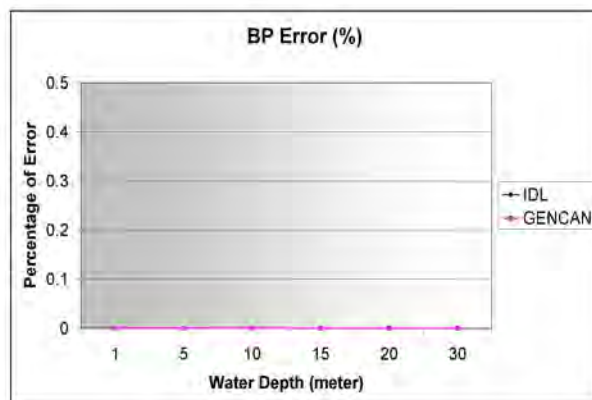


(a)

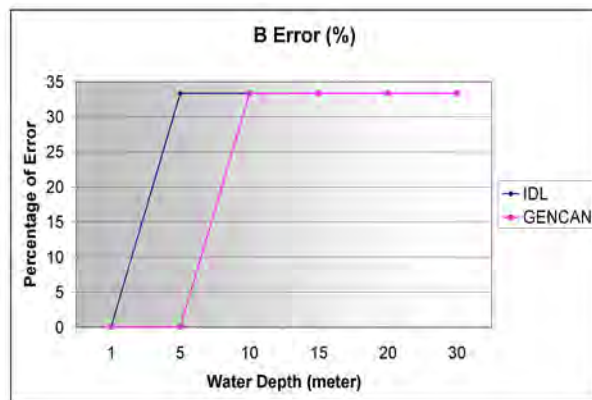


(b)

Figure 4.5: Percent Errors for IDL and GENCAN optimization methods for optically dense water



(a)



(b)

Figure 4.6: Percent Errors for IDL and GENCAN optimization methods for optically dense water, continuation

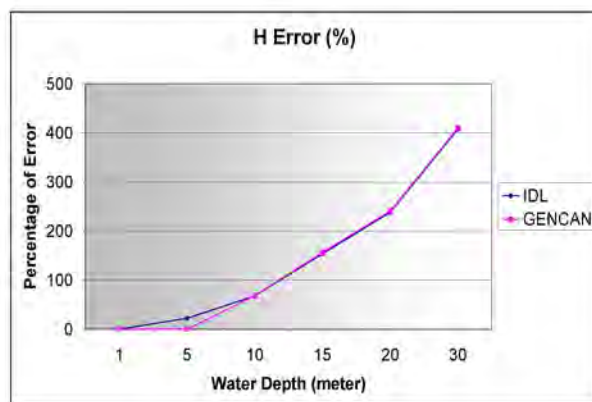
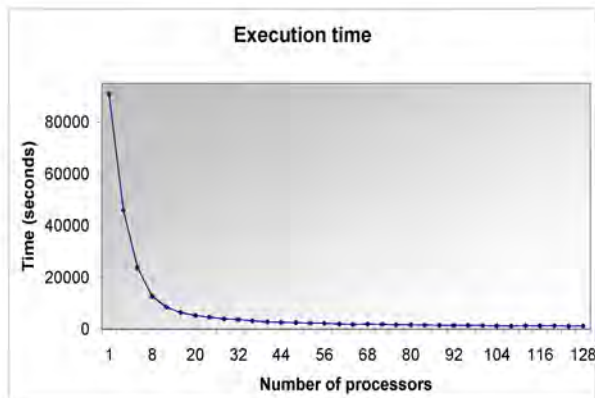


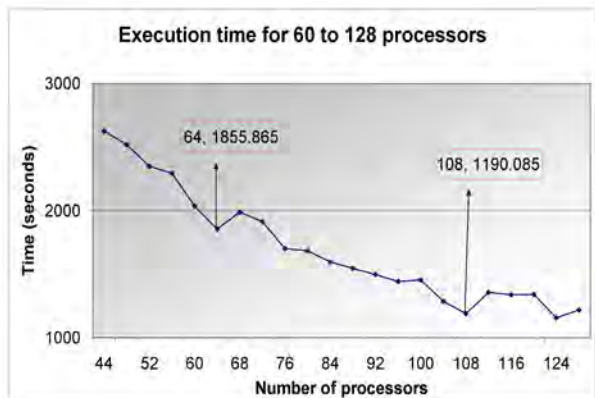
Figure 4.7: Percent Errors for IDL and GENCAN optimization methods for optically dense water, continuation

## 4.4 Performance Results

An experiment with 5120 different samples of nuisance parameters applied to a clear water synthetic vector was carried out to measure execution time and speedup of the parallel implementation of the SAI model.



(a)



(b)

Figure 4.8: Execution time of SAI model for clear water (a); enlarge subset (b)

Figure 4.8(a) shows reduction of the execution time as the number of processors increases. A closer look at the results, Figure 4.8(b), shows that at 64 processors

we obtain the first local minimum time of 1855.86 seconds, which is 2.04% of serial time. At 108 processors the time is 1190.085 seconds, which is 1.31% of serial time. After 108 processors, the execution time continues decreasing, but at slower rate.

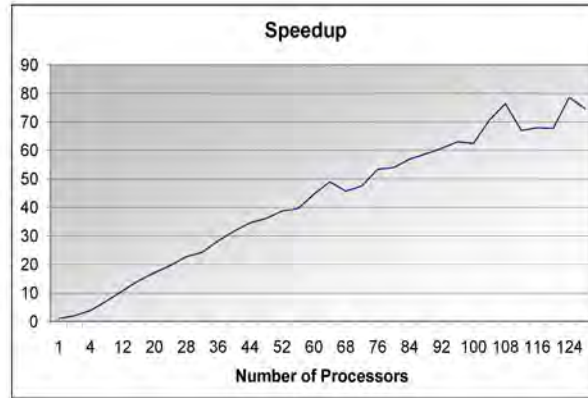


Figure 4.9: Speedup of SAI model for clear water

Figure 4.9 illustrates the speedup obtained as the number of processors increases. A superlinear speedup is not totally obtained, mostly because other processes were running at the same time. The speedup also demonstrates that after 108 processors an overhead occurs. Similar results were observed when the analysis was repeated with an increased number of samples. The results presented here demonstrate the overall performance of the parallel implementation with respect to serial implementation, reducing the total runtime from 20 hours with a single processor to less than 20 minutes with 128 processors. The reduction of the execution time allows the user to work with large sets of data and also performs exhaustive researches that normally require inconveniently long periods of time (hours or days).

# CHAPTER 5

## SENSITIVITY ANALYSIS

This chapter describes the Sobol method used for performing the sensitivity analysis (SA). The methodology for the SA and results obtained for clear and optically dense water are discussed.

### 5.1 Sobol Method

The Sobol method is a variance-based approach [13], [14] that measures the overall and individual interactions at any order effect of the nuisance parameters  $\gamma$  on the variance of the output variables (parameters of interest  $\theta$ ). In this analysis, the output  $\theta$  is equal to a set of  $n$  statistically independent input parameters  $f(\gamma)$ . The last one is decomposed into summands of increasing dimensionality that represents all possible source of variability:

$$\theta = f(\gamma_1, \dots, \gamma_n) = f_0 + \sum_{i=1}^n f_i(\gamma_i) + \sum_{i=1}^n \sum_{j=i+1}^n f_{ij}(\gamma_i, \gamma_j) + \dots + f_{1,\dots,n}(\gamma_1, \dots, \gamma_n), \quad (5.1)$$

where  $f_0$  is the zero order effect equivalent to the mean value of  $f(\gamma)$ , which must be a constant. The effects represented by the functions are:  $f_i$ , the main effect of the  $i$  -  $\gamma$  parameter;  $f_{ij}$ , the second order effect is the interaction effect between parameter  $i$  and  $j$ , and  $f_{1,\dots,n}$ , the larger effect. Then, according to the concept of Analysis Of Variance (ANOVA) decomposition [40], the total variance is defined as:

$$Var(\theta) = \sum_{i=1}^n Var(f_i) + \sum_{i=1}^n \sum_{j=i+1}^n Var(f_{ij}) + \dots + Var(f_{1,\dots,n}). \quad (5.2)$$

The global sensitivity index is defined as the ratio between the conditional expectation variance ( $Var(E(\theta|\gamma_i))$  or  $Var(f_i)$ , the variance of the expectation value of  $\theta$  conditional on a fixed value of  $\gamma$  and the total variance  $Var(\theta)$ , such that:

$$S_i = Var(f_i)/Var(\theta), \quad (5.3)$$

where  $S_i$  is the main sensitivity index and  $S_i \in [0, 1]$ . The second order effect or interaction sensitivity index is defined as:

$$S_{ij} = Var(f_{ij})/Var(\theta), \quad (5.4)$$

and the larger sensitivity indices are:

$$S_{1,\dots,n} = Var(f_{1,\dots,n})/Var(\theta). \quad (5.5)$$

Additionally, all sensitivity indices sum to one:

$$\sum_{i=1}^n S_i + \sum_{i=1}^n \sum_{j=i+1}^n S_{ij} + \dots + S_{1,\dots,n} = 1. \quad (5.6)$$

Following from the previous definition, the Total Sensitivity Index of parameter  $i$  [13], named  $ST(i)$ , is defined as the sum of all sensitivity indices that include the parameter  $i$ ,

$$ST(i) = S_i + S_{ij} + \dots + S_{i,n}, \quad (5.7)$$

or

$$ST(i) = 1 - S_{\sim i}, \quad (5.8)$$

where  $S_{\sim i}$  is the sum of all sensitivity indices not including parameter  $i$ . Chan et al. [13] consider  $ST(i)$  an important value because it quantitatively ranks the influence of nuisance parameters on the parameters of interest. Thus, if the  $ST$  of a factor is negligible, then the factor is considered non-influential and its value can be fixed to any value within its specified range of variability. Otherwise, the factor has to be considered important and the user has to pay attention to the value that this factor is assigned (examples of  $ST$  are shown in [13] and [24]).

## 5.2 Methodology

We propose to follow four steps, described in Figure 5.1, to accomplish the SA:

1. Define the range and distribution function for each of the input variables (i.e. the nuisance parameters). In this study, an uniform distribution function was selected for all variables.
2. Generate samples of the nuisance parameters. The choice of the sampling method depends on the type of sensitivity analysis that will be performed. The Sobol method was used in this study to generating the samples. The user has to specify the conditions, like first and total order calculation or has the option of choosing other orders, but always including total order calculation. Depending on the order number, the number of executions (samples) will increase. In this research, second order was chose using Sobol method, as result 5120 samples are generated. The generation of samples is not time consuming.
3. The model is fed with the samples. In our case, the samples were exported and read by the C++/MPI program. Implementation then included generating the synthetic vectors using forward model, and subsequently performing the actual inversion. Output from this step are the parameters of interest derived for each set of samples.

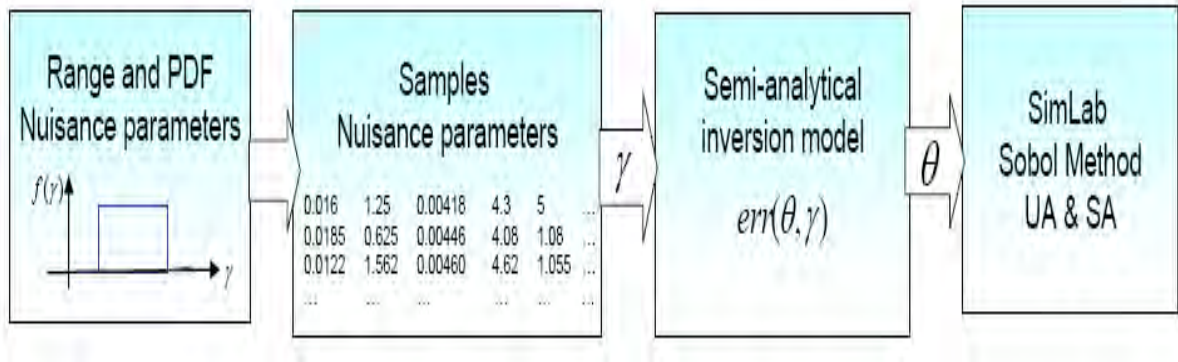


Figure 5.1: Steps to accomplish the Sensitivity Analysis

4. Perform the uncertainty and sensitivity analysis. The results of the parallel implementation of the inversion model are imported to SimLab for analysis.

Note that steps (1) and (2) are performed using the SimLab Statistical Preprocessor module; step (3) is performed external to SimLab using C++/LAM-MPI; and the final step (4) is performed using the SimLab Statistical Postprocessor module.

SimLab [24] was primarily designed for Monte Carlo Analysis. However, this software has the flexibility to work with other models, even if the model is in another computational infrastructure, such as the SAI model used here, and the results can be exported to perform the SA.

## 5.3 Results

The uncertainty analysis (UA) and sensitivity analysis (SA) for both clear and optically dense water are discussed in this section.

### 5.3.1 Results for Clear Water

The uncertainty analysis (UA) performed in step (4) of the above procedure investigates the uncertainty in the parameters of interest according to variability in

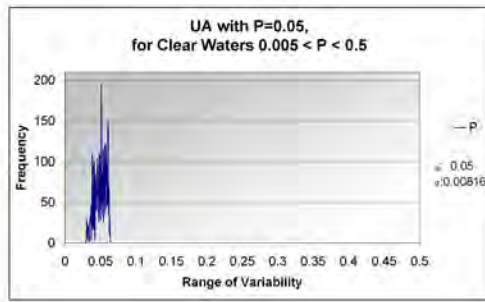
the nuisance parameters [24]. Figure 5.2 is an example of the UA for clear water with the initial values of  $P=0.05$ ,  $G=0.05$ ,  $BP=0.01$ ,  $B=0.4$ , and  $H=5$ . The results exhibit little variance, and the mean value is close to those used as initial values in the forward model. At water depth greater than 10 meters (Figure 5.3), some parameters start showing variations, which are due to the nuisance parameters.

To find out how influential the individual nuisance parameters are, the SA is carried out. The SA results indicate which nuisance parameters are most influential and thus which parameters need to be properly assigned so as to lower uncertainty in the output and improve model performance.

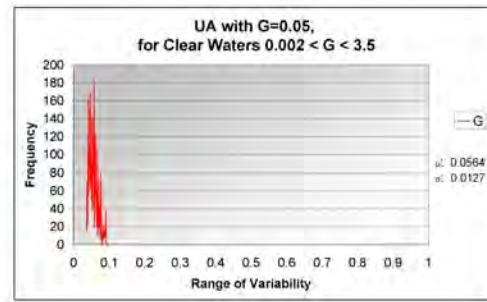
Table 5.1 summarizes the sensitivity indices (percentage) of the first and second order effects, showing only the most representative values. The results are for clear water with  $H$  set to 1,5,10,15,20, and 30 meters. The analysis was performed using two separate tests:

- Sobol method, first order only (Sobol1), with 1792 samples
- Sobol method, first and second order (Sobol4), with 5120 samples

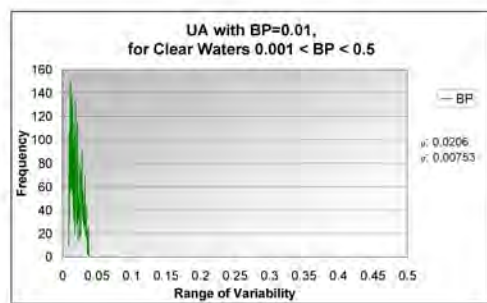
Sensitivity indices for these tests are evaluated according to the following [13]: 100-80 %:very important, 80-50 %:important, 50-30 %:unimportant, and 30-0 %:irrelevant.



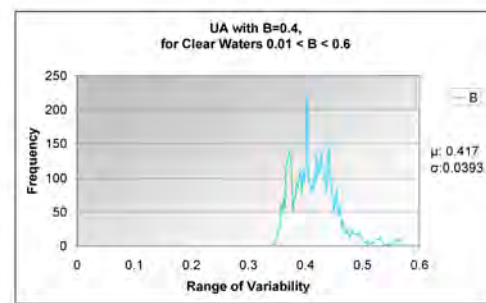
(a)



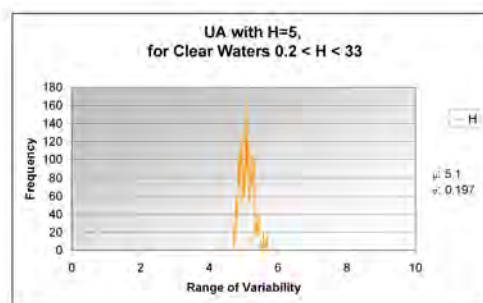
(b)



(c)

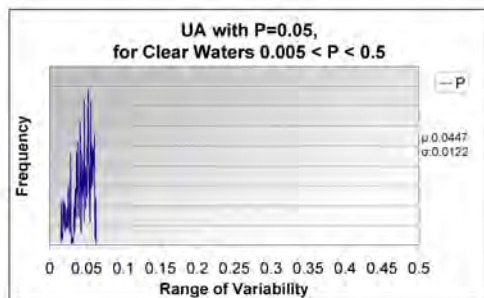


(d)

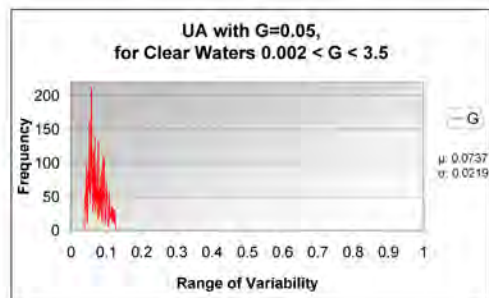


(e)

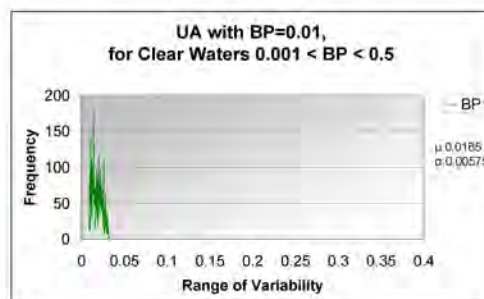
Figure 5.2: Results of uncertainty analysis for clear water at 5 meters



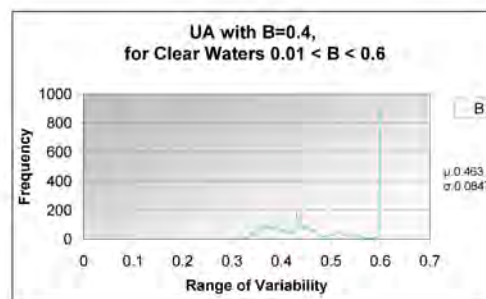
(a)



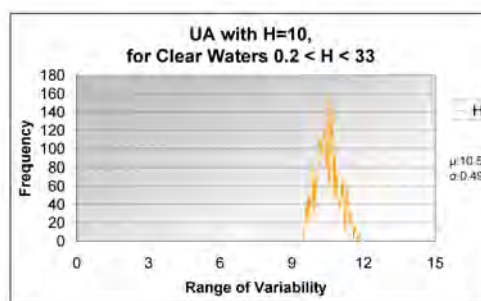
(b)



(c)



(d)



(e)

Figure 5.3: Results of uncertainty analysis for clear water at 10 meters

Table 5.1: Results for Clear Water with different water depths, H

<b>H (m)</b>	<b>Test</b>	<b>P</b>	<b>G</b>	<b>BP</b>	<b>B</b>	<b>H</b>
1	Sobol1	S(95.36)	S(99.87)	Y(86.46)	$\zeta$ (94.10)	$D_{op}$ (85.95)
	sobol4	S(100)	S(100)	Y(89.66)	$\zeta$ (89.2)	$D_{op}$ (91.79)
5	Sobol1	S(89.8)	S(66.89) Y(30.75)	Y(94.17)	S(47.94) $\zeta$ (39.12)	$D_{op}$ (53.55) S(30.37)
	Sobol4	S(96.14)	S(70.03)	Y(95.3)	S(56.53) $\zeta$ (36.77)	$D_{op}$ (54.45) S(29.51)
10	Sobol1	S(67.68) Y(27)	Y(75.44) S(24.79)	Y(91.11)	S(64.15) Y(13.87)	$D_{op}$ (38.73) Y(27.29)
	Sobol4	S(70.97) Y(30.06)	Y(80.89) S(25.89)	Y(89.76)	S(69.87) Y(22.17)	$D_{op}$ (45.62) S(30.45)
15	Sobol1	S(68.31)	Y(84.45) S(15.82)	Y(89.57)	S(46.76) Y(28.57)	S(53.59) $D_{op}$ (14.97)
	Sobol4	S(72.30) Y(25.79)	Y(89.33) S(16.87)	Y(86.78)	S(54.49) Y(29.86)	S(52.5) $D_{op}$ (18.65)
20	Sobol1	S(80.09)	Y(81.24) S(18.28)	Y(91.05)	$D_{op}$ (21.14) S(20.66)	S(73.80)
	Sobol4	S(85.21) S,Y(13.66)	Y(86.30) S(19.70)	Y(89.79)	S(28.89) S,Y(11.73)	S(79.29) S,Y(18)
30	Sobol1	S(84.79)	Y(75.11) S(22.79)	Y(92.17)	S(86.10)	Y(30.47) S(23.97)
	Sobol4	S(90.53) S,Y(18)	Y(79.19) S(24.44)	Y(92.35)	S(95.25)	Y(32.64) S(27.87)

Observations from examining the results in Table 5.1 include:

*H = 1 meter:* Sobol4, with more samples, has more stability and accuracy than Sobol1. The values for all second order interactions (on the order of 1% or less) are not very significant.

*H = 5 meters:* Results are similar to those obtained at 1 meter, except for B, where S replaces  $\zeta$  as the most influential parameter.

*H = 10 meters:* Additional parameters and relationships are emerging. The nuisance parameter Y replaces S as the important parameter for G;  $\zeta$  is no longer influent on B; and  $D_{op}$  remains the most influential parameter for H, but with a score less than 50%, which indicates it is unimportant.

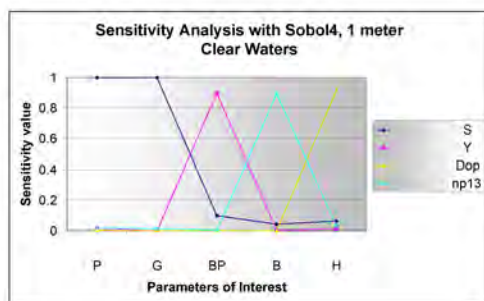
*H = 15 meters:* Results are similar to those at 10 meters, except for H, where S is now the most significant nuisance parameter.

*H = 20 meters:* The parameters P,G, and BP exhibit the same behavior as at 15 meters. For parameter B, there are no significant nuisance parameters, likely because the increasing depth is adding difficulty for resolving information about the bottom.

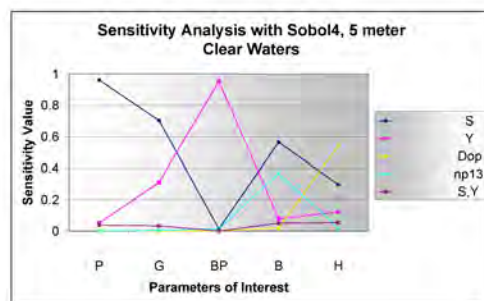
*H = 30 meters:* The nuisance parameters for P,G, and BP show equal or higher values as at 20 meters; S again becomes the most significant parameter for B; and there are no important parameters for H.

A summary of the effects presented in Table 5.1 for the sensitivity analysis of clear water are shown in Figure 5.4. Here, the sensitivities are presented on a scale from 0 to 1, where 0 represents 0% of influence, and 1 represents 100% of influence over the parameter of interest. Figure 5.4 show that the nuisance parameter S is consistent for parameter P; also S appears as influential to parameter G, but for depths up to 5 meters Y is the most influential nuisance parameter. The parameter Y is presented as the only one influential over the parameter of interest BP. The parameter of interest B is affected for several parameters as the water depth increase and S is the more influential nuisance parameter showed. The parameter of interest H presents great variability in its sensitivity analysis, with different nuisance parameters emerging such as S, Y and  $D_{op}$ , dependent on the water depth.

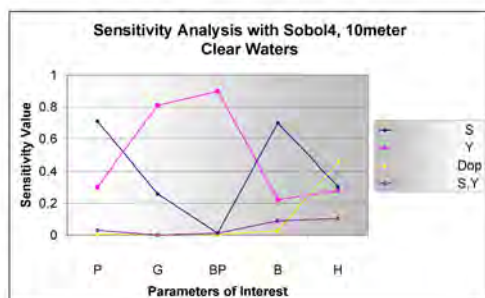
As shown in Figure 5.4, the first and second order analysis do not always clearly indicate which parameters are the most important. For example, it is not clear which nuisance parameter is most influential on water depth, H. However, the *ST* index may help clarify and resolve this question. Figure 5.5 shows the total sensitivity indices for parameter H at 30 meters. It is clear from this figure that Y is the most significant nuisance parameter, followed by S. Parameters such as np5, np6,  $D_o$ ,  $D_1$ ,



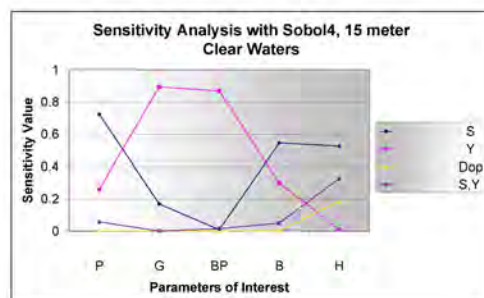
(a)



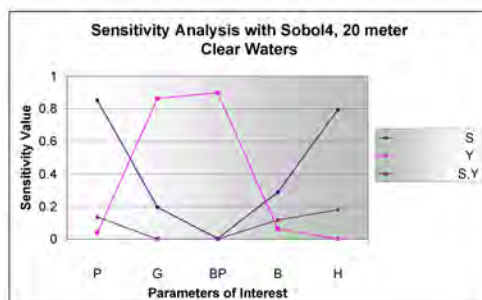
(b)



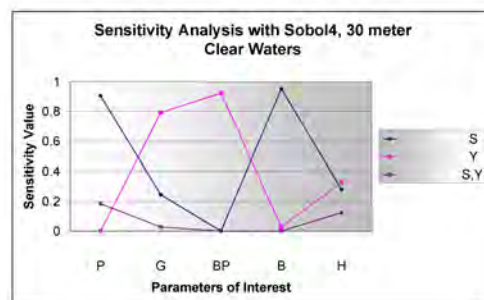
(c)



(d)



(e)



(f)

Figure 5.4: Main results of the sensitivity analysis for clear water

$D_{1p}$ ,  $g_1$ ,  $\zeta$  (represented in the figures as np13),  $\Gamma$  (represented in the figures as np14), and  $g_o$  have  $ST$  indices close to zero and are thus not important for determining  $H$ .

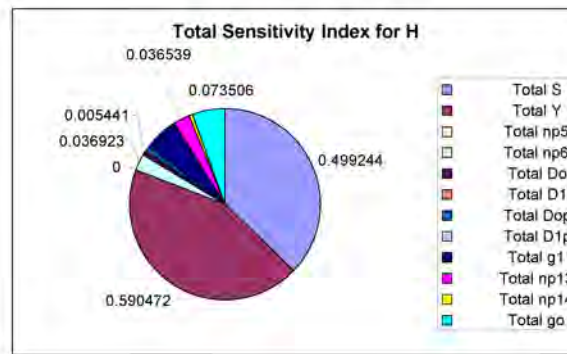


Figure 5.5: Results of total sensitivity index for parameter H for clear water at 30 meters depth

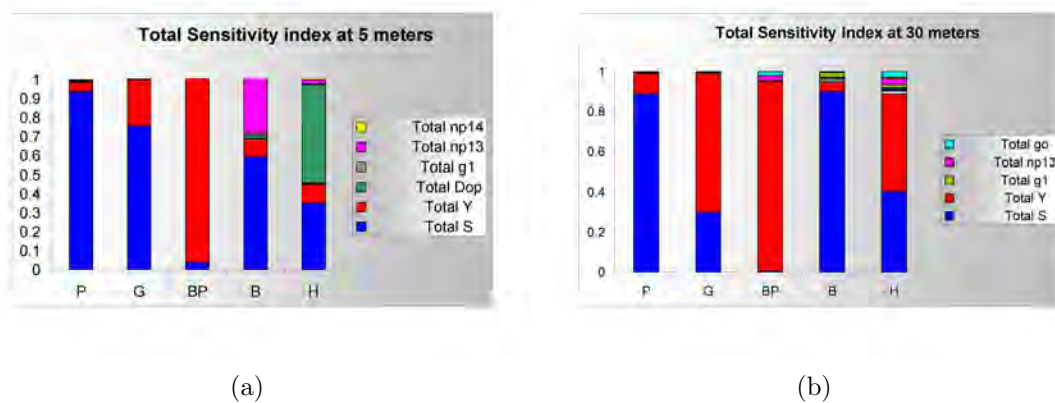


Figure 5.6: Results of total sensitivity index for clear water at 5 and 30 meters depth

As another way of looking at the same data, Figure 5.6 illustrates the relative influence of S and Y on the different parameters of interest at 5 and 30 meters depth. Figure 5.6(a) shows that S strongly influence two parameters, P and G, with also influence in parameter B, and Y has strongly influence in the parameters BP. For parameter H there are two nuisance parameters with influence  $D_{op}$  and S, but this happen up to 5 meters, because at 30 meters, in Figure 5.6(b), as was mentioned before the most influence nuisance parameter is Y. Also, there is a change in parameter G at 30 meters, where S is not the most important, instead we have Y as

the most influential. Thus, the parameters S and Y are more significant to P and G. In this case, S represents spectral information related to Gelbstoff, and Y represents spectral information for particle backscattering. A change in the concentration of the particles in the water will affect what can be retrieved from it, thus the absorption of phytoplankton (P) and Gelbstoff (G) will vary too. These results are in agreement with indications from Lee et al. [2] that S and Y directly influence P and G values.

S and Y also influence other parameters. The parameter Y is the only parameter of those tested responsible for changes in BP.  $\zeta$  and S emerge with increasing water depth as the parameters that affect B. Up to 10 meters, the distribution function of scattered photon from bottom,  $D_{op}$ , is the dominant parameter affecting H, but at 15 and 20 meters, S is important, and at 30 meters, it is replaced by Y.

### 5.3.2 Results for Optically Dense Water

The uncertainty analysis for optically dense reveals much greater uncertainty in the parameters of interest particularly with increasing water depth. This is attributed to much greater scattering and absorption present in this water type and hence lower available signal for model processing (i.e., lower values of  $L_d$ , downwelling radiance). Figure 5.7, shows the UA at 5 meters depth for optically dense water (P=0.4, G=1, BP=0.2, B=0.4, and H=5). Note the much greater uncertainty shown in Figure 5.7 than for clear water at 5 meters depth as shown in Figure 5.2.

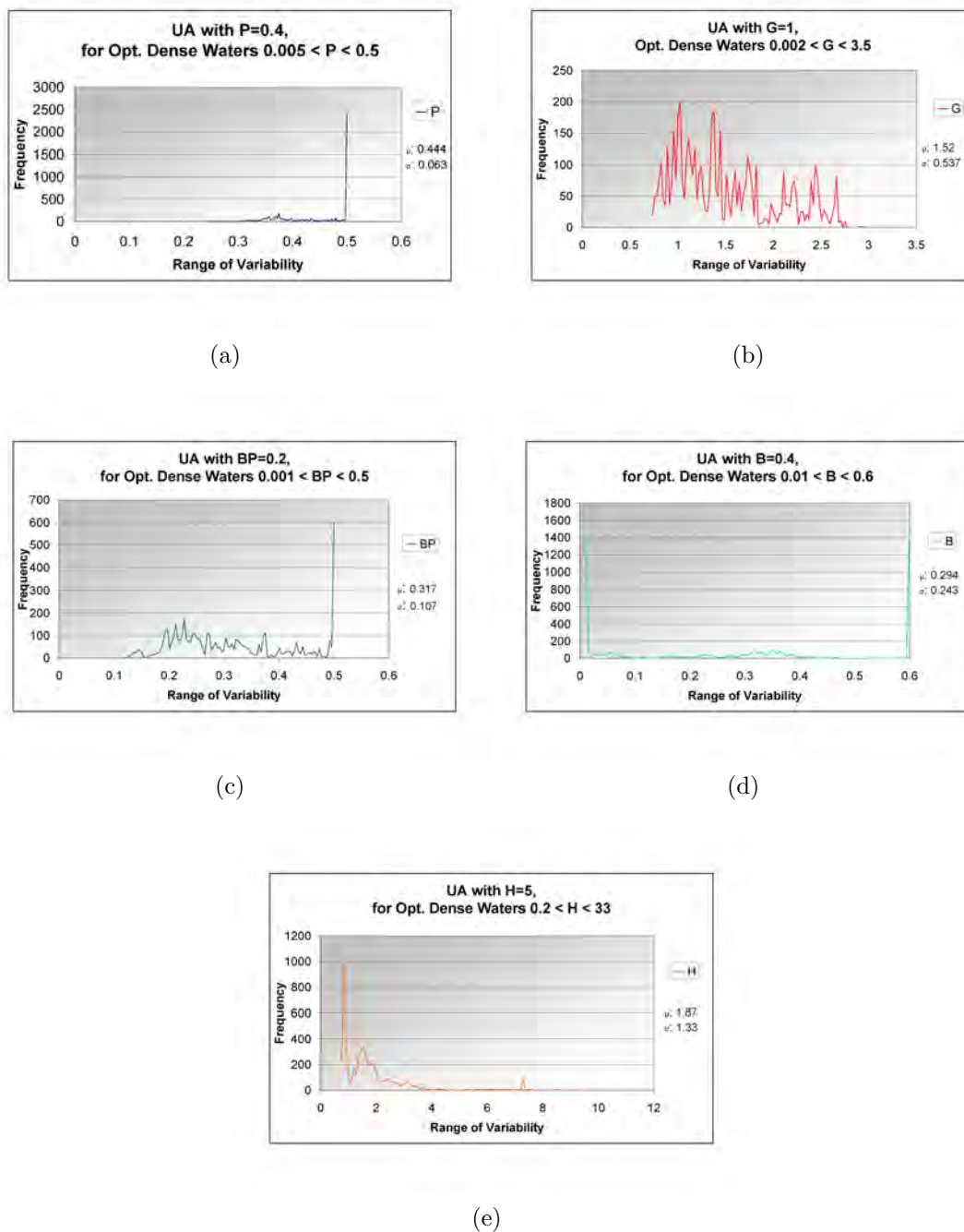


Figure 5.7: Results of uncertainty analysis for optically dense water at 1 meter

Table 5.2 presents the sensitivity indices (percentage) of the first and second order analyses for optically dense water with varying water depth ( $H=1,5,10,15,20,30$  meters). AS with the clear water results, the same number of samples are used for

Table 5.2: Results for Optically Dense Water with different depths, H

<b>H(m)</b>	<b>Test</b>	<b>P</b>	<b>G</b>	<b>BP</b>	<b>B</b>	<b>H</b>
1	Sobol1	Y(46.20) S(5.99)	S(77.19) Y(6.22)	S(63.28) Y(7.06)	S(67.48) $\zeta$ (12.86)	Y(60.56) S(8.52)
	sobol4	S,Y(57.82) Y(35.00)	S(74.26) S,Y(22.70)	S(63.46) S,Y(32.85)	S(79.88) $\zeta$ (17.40)	Y(49.31) S,Y(32.75)
5	Sobol1	S(5.00)	S(54.35) Y(21.68)	S(43.57) Y(30.75)	S(62.94) $\zeta$ (8.50)	S(18.37) g1(6.47)
	Sobol4	S,Y(67.26)	S(56.27) S,Y(27.99)	S(41.98) S,Y(34.34)	S(68.41) S,Y(17.65)	S(26.36) S, $\zeta$ (18.23)
10	Sobol1	S(5.07)	S(54.37) Y(21.67)	S(43.56) Y(30.76)	S(61.17) Y(7.74)	S(21.74) g1(8.44)
	Sobol4	S,Y(67.30)	S(56.3) S,Y(28.03)	S(41.99) S,Y(34.32)	S(68.46) S,Y(17.65)	S(36.26) S, $\zeta$ (16.26)
15	Sobol1	S(5.07)	S(54.37) Y(21.66)	S(43.55) Y(30.76)	S(61.29) $\zeta$ (7.52)	S(19.36) g1(7.56)
	Sobol4	S,Y(67.23)	S(56.29) S,Y(28.03)	S(41.99) S,Y(34.32)	S(73.08) Y(15.53)	S(28.15) S, $D_{1p}$ (16.19)
20	Sobol1	S(5.07)	S(54.37) Y(21.66)	S(43.56) Y(30.76)	S(63.39) $\zeta$ (7.91)	S(22.85) g1(7.51)
	Sobol4	S,Y(67.23)	S(56.29) S,Y(28.03)	S(41.99) S,Y(34.32)	S(68.46) Y(17.64)	S(33.25) S, $\zeta$ (11.35)
30	Sobol1	S(5.07)	S(54.37) Y(21.66)	S(43.56) Y(30.76)	S(63.28) $\zeta$ (8.52)	S(20.64)
	Sobol4	S,Y(67.25)	S(56.30) S,Y(28.00)	S(41.99) S,Y(34.32)	S(72.66) S,Y(13.43)	S(32.89) $\Gamma$ (17.96)

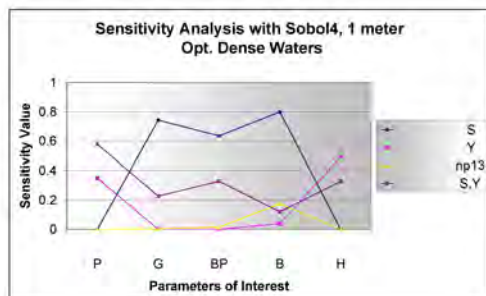
the two different Sobol test, and only the most significant values are shown in Table 5.2.

Observations derived from examining the results in Table 5.2 include:

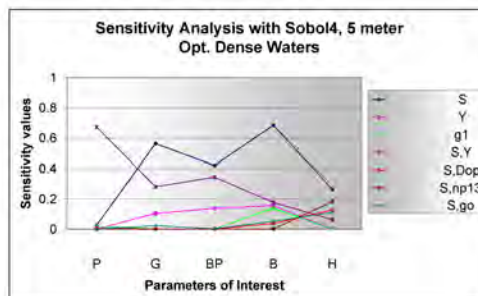
*H = 1 meter:* Parameters S and Y are again the most influential parameters. The nuisance parameter S is the most influential for parameters G, BP and B, for both the Sobol1 and Sobol2 tests. For the parameters of interest P and H, the parameter Y is the most influential in the Sobol1 test. However, in the Sobol2 test the second order index S,Y is the most significant for parameter P with 57.82%.

*H = 5, 10, 15, 20 and 30 meters:* The results are nearly identical to those at 1 meter. Except for BP and H, whose nuisance parameters all have values less than 50% and are thus considered unimportant. However, all note that overall model accuracy is poor for optically dense water at these depths.

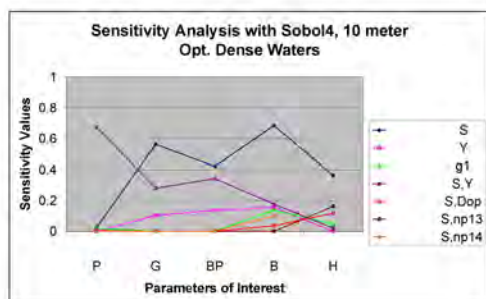
The results of the sensitivity analysis for first and second order effect in optically dense water are illustrated in Figure 5.8. As with Figure 5.4 for clear water, the results were plotted using a scale of 0 to 1. Figure 5.8 shows the importance of S in the uncertainty of estimating the parameters of interest G, BP, B and H, except for H at 1 meter, Figure 5.8(a), which is affected in this case by the nuisance parameter Y. The parameter P appears be influenced by the second order index S,Y at all different water depths.



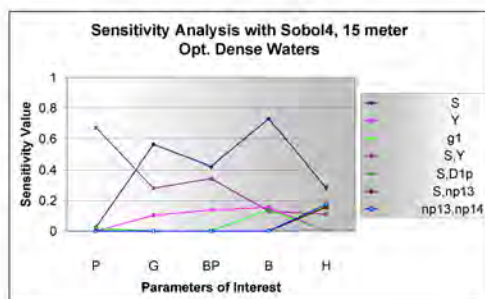
(a)



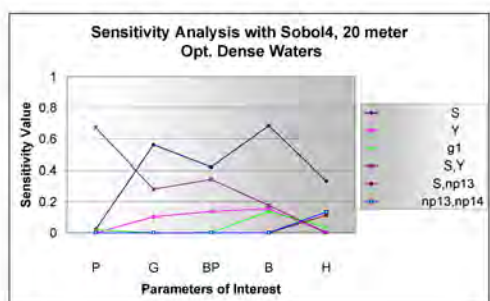
(b)



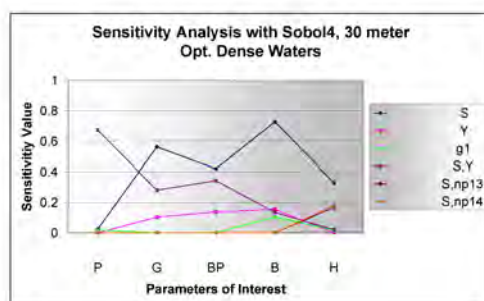
(c)



(d)



(e)



(f)

Figure 5.8: Principal results of sensitivity analysis for optically dense water

Figure 5.9 shows the total sensitivity indices for S and Y at 5 meters, which are the only parameters with significant influence in optically dense water. All other parameters such as  $np5$ ,  $np6$ ,  $D_o$ ,  $D_1$ ,  $D_{op}$ ,  $D_{1p}$ ,  $g_1$ ,  $\zeta$ ,  $\Gamma$ , and  $g_o$  were found to be unimportant. According to Figure 5.9(a), S is the most significant nuisance parameter for all five parameters of interest and Y is second, except for P where S and Y have nearly equal influence. Similar results are also observed at 30 meters depth, Figure 5.9(b), where the nuisance parameters S and Y are again the most influential.

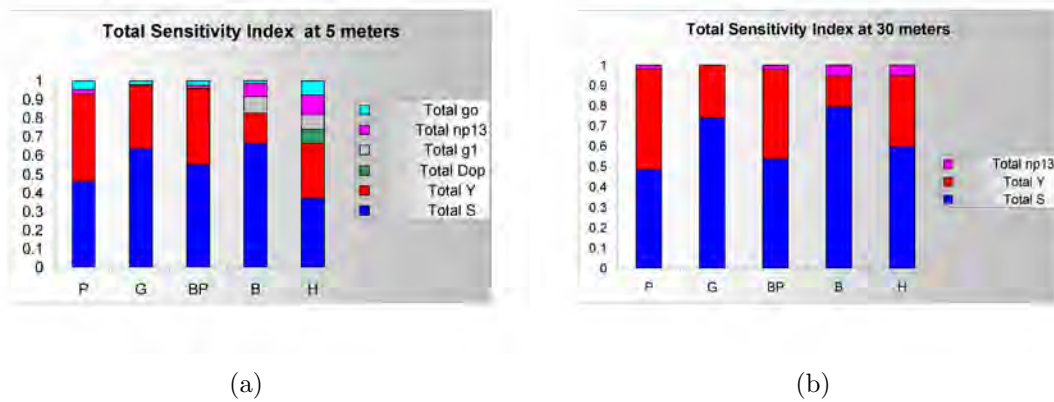


Figure 5.9: Results of total sensitivity index for optically dense water at 5 and 30 meters depth

As shown in Figure 5.10(b), there are also instances where S,Y (second order effect) have greater influence than the individual parameters (first order effects, Figure 5.10(a)). For example, at 5 meters depth the parameter S (5%) is the most influential parameter on P in the first order test (sobol1), while in the combined first and second order test (sobol4), the first order effects become negligible and S,Y (67.26%) become the most significant. Values at depths over 5 meters exhibit similar results which is indicative of the problem that it is more difficult to retrieve information about the bottom and water column in optically dense water at greater depths.

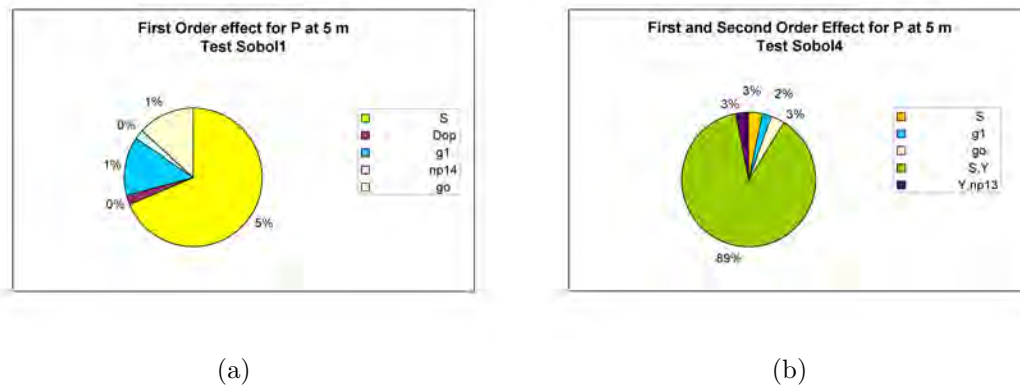


Figure 5.10: Comparison of first and second order effects for optically dense water at 5 meters depth

In conclusion it is necessary to clarify some physical aspects that interfered with the successful gathering of benthic information and subsequent sensitivity analysis. Downwelling radiation is significantly impacted by absorption and scattering in the water column, which is a function of the water itself and its constituents. This result in an exponential decrease in radiation with increasing water depth. Additionally, there are other factors that can affect the energy transmitted or reflected such as the solar geometry and water surface conditions but they are not directly considered in this study. Another factor affected by the reduction in radiation is the retrieval of bottom albedo in the shallow water, which is obtained with difficulty because not enough energy can arrive at the bottom to be reflected and thus registered by the sensor. The effects of absorption and scattering are less significant in clear water and more significant in optically dense waters, and thus our ability to extract information describing the benthic substrate is limited by the amount of energy available to be reflected from the bottom.

# CHAPTER 6

## CONCLUSIONS AND FUTURE WORKS

### 6.1 Conclusions

The contributions of this thesis are related to the parallel implementation of the SAI model as well as the use of a sensitivity analysis to identify the most influential nuisance parameters within the model. The GENCAN routine was used to implement the SAI model for case of clear and optically dense water. In case of clear water GENCAN results yielded less than 1% of error, compared with the implementation done in IDL/ENVI, where errors ranged from 1% to 200% of error depending on the parameter. An exception appears when calculating bottom albedo (B) and water depth (H) at 30 meters using GENCAN, for which the errors are 23.12% and 4.91%, respectively. In case of optically dense water, for both GENCAN and IDL/ENVI results yielded less than 1% of error for phytoplankton absorption (P), Gelbstoff absorption (G) and Backscattering by particles (BP) at all water depth. Again an exception appears for parameters B and H; for B GENCAN presents an error of 33.33% from 10 meters and IDL/ENVI presents 33.33% error after 5 meters; for H, GENCAN presents an increasing error from 68.29% to 409.81 at 10 meters to 30 meters, and IDL presents an increasing error from 22.44% to 409.81% at 5 meters to 30 meters. These errors occur because the effects of absorption and scattering increase at deeper waters and more with optically dense water, significantly increasing the difficulty of retrieving the parameters. However, the trade-off for using GENCAN

to get more accurate results is that the model operates at a higher computational cost.

The parallel implementation of the SAI model using C++/LAM-MPI provided the computation power for addressing a complex optimization and sensitivity analysis. The performance results show a substantial reduction in the execution time. With 64 processors the execution time for an experiment with 5120 samples was around 1855.86 seconds, which is only 2.04% of the sequential time.

In terms of the sensitivity analysis results of first order effect, second order effects, and total sensitivity index were examined. The first order analysis permitted analyzing the effects of the parameters individually, where only one or two nuisance parameters were found influential for each parameter of interest. In the case of clear water, the influential nuisance parameters were: S for P, G, B, and H; Y for P, G, BP, and H;  $\zeta$  for B, and  $D_{op}$  for H. However, these results also varied with water depth. In the case of optically dense waters, the most influential nuisance parameters found were: S for G, BP; and B, and Y for H. These outputs are even more affected by the water depth, where increasing depth produce significantly higher absorption of the light. Second order effects allowed the effect of the combination of two parameters to become apparent. In case of clear waters these effects were classified as not significant. However, in case of optically dense waters these effects are important for parameter P, which is affected by S,Y. The total sensitivity index helped to corroborate and clarify the results. For example, S was found to be the most influential nuisance parameter on BP, for which first and second order effect results are not significant. The influence of parameters S and Y prove the importance of variations in water composition related to gelbstoff, chlorophyll, and suspended particles, which impact scattering and absorption. The suspended particles affect the scattering effect and the gelbstoff and chlorophyll affect the absorption coefficient.

The parallel implementation was a great contribution and a good beginning for investigations that require operate over large set of data and perform complex optimization. Also, it was done a progress in the study and sensitivity analysis of SAI model, because an analysis of many nuisance parameters at the same time and with a lot of definition of samples for them were not done before. Thus, now there is a more complete study of the SAI model, leaving the door open to more improvements of this model.

## 6.2 Future work

The OOI library offers three different methods to achieve an optimization. We only applied one of them, GENCAN that was tested and show excellent results despite of the time consuming. The other two optimization methods are spg (spectral projected gradient) and pgrad (projected gradient) methods. A future study can be conducted to compare and see which of these methods show good performance results as much as lower time consuming.

In this thesis, a sensitivity analysis was performed. The results obtained are considered a first step in the improvement of the SAI model. After now identifying the most influential nuisance parameters more specific studies can be used to improve the selection of values for these parameters and thus increase model performance. Furthermore, the parallel implementation can be utilized to greatly improve processing speed.

## REFERENCE LIST

- [1] Z.P. Lee, K. L. Carder, C.D. Mobley, R. G. Steward, and J. Patch. Hyperspectral remote sensing for shallow waters. 1. a semianalytical model. *Applied Optics*, Vol. 37:6329–6338, 1998.
- [2] Z.P. Lee, K. L. Carder, C.D. Mobley, R. G. Steward, and J. Patch. Hyperspectral remote sensing for shallow waters. 2. deriving bottom depths and water properties by optimization. *Applied Optics*, Vol. 38:6329–6338, 1998.
- [3] MicroImages Inc. <http://www.microimages.com/getstart/introrse.htm>. *Introduction to Remote Sensing of Environment (RSE)*, 2001.
- [4] G. A. Shaw and H. K. Burke. Spectral imaging for remote sensing. *Lincoln Laboratory Journal*, Vol. 14, Number 1:3–28, 2003.
- [5] J. A. Goodman. *Hyperspectral remote sensing of coral reefs: deriving bathymetry, aquatic optical properties and a benthic spectral unmixing classification using AVIRIS data in the Hawaiian Islands*. PhD thesis, University of California, Davis, 2004.
- [6] Blaise Barney. Introduction to parallel computing, [http://www.llnl.gov/computing/tutorials/parallel\\_comp](http://www.llnl.gov/computing/tutorials/parallel_comp), 2006.
- [7] Z.P. Lee, K. L. Carder, and C.O. Davis. Using hyperspectral imaging to characterize the coastal environment. *IEEE Aerospace Conference*, pages 1515–1521, 2002.
- [8] H. R. Gordon, O. B. Brown, and M. M. Jacobs. Computed relationships between the inherent and apparent optical properties of a flat homogeneous ocean. *Applied Optics*, Vol. 14, vol. 14:417–428, 1975.

- [9] C. D. Mobley and L. K. Sundman. *Hydrolight 4.2 users guide*. Sequoia Scientific Inc., Redmon, WA, second edition, 2001.
- [10] Interactive Data Language. <http://rsinc.com/idl/>.
- [11] Environment for Visualizing Images. <http://www.ittvis.com/envi/index.asp>.
- [12] J. Goodman and S. Ustin. Airborne hyperspectral analysis of coral ecosystems in the hawaiian islands. *Proceedings 30th International Symposium on Remote Sensing of Environment*, 2003.
- [13] K. Chan, A. Saltelli, and S. Tarantola. Sensitivity analysis of model output: Variance-based methods make the difference. *Proceeding of the 1997 Winter Simulation Conference*, pages 261–268, 1997.
- [14] European Commission - IPSC. *SimLab 2.2 - Reference Manual* <http://simlab.jrc.cec.eu.int/>, 2004.
- [15] W. Lugo-Beauchamp, C. Carvajal-Jimenez, and W. Rivera. Performance of hyperspectral imaging algorithms on IA-64. *Proceedings IASTED International Conference on Circuits, Signals, and Systems*, pages 327–332, 2004.
- [16] K. A. Hawick and H. A. James. Distributed high-performance computing for remote sensing. *Proceedings of the ACM/IEEE Conference on Supercomputing*, 1997.
- [17] D. Valencia, A. Plaza, P. Martínez, and J. Plaza. On the use of cluster computing architectures for implementation of hyperspectral images analysis algorithms. *Tenth IEEE symposium on computers and communications ISCC*, pages 995–1000, 2005.
- [18] M. Snir, S. Otto, S. Huss-Lederman, D. Walker, and J. Dongarra. *MPI The Complete Reference. Volume 1 - The MPI-1 Core*. The MIT Press, second edition, 1998.

- [19] G. Burns, R. Daoud, and J. Vaigl. LAM: An open cluster environment for MPI. *Proceedings of supercomputing Symposium*, <http://www.lam-mpi.org/download/files/lam-papers.tar.gz>, pages 379–386, 1994.
- [20] J. B. Campbell. Introduction to remote sensing. *The Guilford Press*, 1994.
- [21] M. Wang and S. W. Bailey. Correction of sun glint contamination on the seawifs ocean and atmosphere products. *Applied Optics*, Vol. 40:4790–4798, 2001.
- [22] C. D. Mobley. *Light and Water, Radiative transfer in natural waters*. <http://curtismobley.com/>, 2004.
- [23] A. Saltelli. Global sensitivity analysis an introduction. *Tutorial Lecture for the International Conference on Sensitivity Analysis*, 2004.
- [24] A. Saltelli, S. Tarantola, F. Campolongo, and M. Ratto. *Sensitivity Analysis in practice, A guide to assessing scientific models*. John Wiley & sons, third edition, 2004.
- [25] N. Oreskes, K. Shrader-Frechette, and K. Belitz. Verification, validation, and confirmation of numerical models in earth sciences. *Science*, Vol. 263:641–646, 1994.
- [26] J. M. Duarte-Carvajalino. Sensitivity analysis of the water column effect on the remote sensing reflectance, the shallow waters case. Master’s thesis, University of Puerto Rico, Mayagüez, 2003.
- [27] W. Gropp, E. Lusk, and A. Skjellum. *Using MPI: Portable Parallel Programming with the Message Passing Interface*. MIT Press Cambridge, MA, USA, 1996.
- [28] Z.P. Lee, K. L. Carder, T. G. Peacock, C. O. Davis, and J. L. Mueller. Method to derive ocean absorption coefficients from remote-sensing reflectance. *Applied Optics*, Vol. 35 No. 3:453–462, 1996.
- [29] H. R. Gordon, O. B. Brown, R. H. Evans, J. W. Brown, R. C. Smith, K. S. Baker, and D. K. Clark. A semianalytic radiance model of ocean color. *J.*

- Geophys*, 1988.
- [30] A. Bricaud, A. Morel, and L. Prieur. Absorption by dissolved organic matter of the sea (yellow substance) in the uv and visible domains. *Limnol. Oceanogr.*, Vol. 26:43–53, 1981.
- [31] M. S. Twardowski, E. Boss, J. M. Sullivan, and P. L. Donaghay. Modeling the spectral shape of absorption by chromophoric dissolved organic matter. *Marine Chemistry*, Vol. 89:69–88, 2004.
- [32] K. L. Carder, R. G. Steward, G. R. Harvey, and P. B. Ortner. Marine humic and fulvic acids: Their effects on remote sensing of ocean chlorophyll. *Limnol. Oceanogr.*, Vol. 34(I):68–81, 1989.
- [33] S. C. Liew, A. S. Chia, K. H. Lim, and L. K. Kwoh. Modeling the reflectance spectra of tropical coastal waters. *Proceedings SPIE*, Vol. 4488B:248–255, 2001.
- [34] R. C. Smith and K. S. Baker. Optical properties of the clearest natural waters (200-800 nm). *Applied Optics*, 20:177–184, 1981.
- [35] R. M. Pope and E. S. Fry. Absorption spectrum (380-700 nm) of pure water. 2. integrating cavity measurements. *Applied Optics*, Vol. 36:8710–8723, 1997.
- [36] P. S. Pacheco. *Parallel Programming with MPI*. Morgan Kaufmann, 1996.
- [37] L. D’Áfonseca, R. Biloti, and S. Ventura. Open optimization library. [web page] <http://ool.sourceforge.net/>, 2005.
- [38] E. G. Birgin and J. M. Martínez. Large-scale active-set box-constrained optimization method with spectral projected gradients. *Computational Optimization and Applications*, Vol. 23, Number 1:101–125, 2002.
- [39] E. G. Birgin, J. M. Martínez, and M. Raydan. Spg: Software for convex-constrained optimization. *ACM Transactions on mathematical software*, Vol. 27:340–349, 2001.

- [40] W. Chen and R. Jin. Analytical variance-based global sensitivity analysis in simulation-based design under uncertainty. *ASME Design Automation Conference*, 2004.